

**GEORGIA DOT RESEARCH PROJECT 1315**

**FINAL REPORT**

**ASSESSMENT OF SAND QUALITY ON CONCRETE  
PERFORMANCE: EXAMINATION OF ACIDIC AND  
SULFATE/SULFIDE-BEARING SANDS**



**OFFICE OF RESEARCH**

GDOT Research Project No. RP 1315

Final Report

ASSESSMENT OF SAND QUALITY ON CONCRETE PERFORMANCE:  
EXAMINATION OF ACIDIC AND SULFATE/SULFIDE-BEARING SANDS

By  
Alvaro Paul  
Kimberly E. Kurtis  
Lawrence F. Kahn  
Preet M. Singh

Georgia Institute of Technology

Contract with

Georgia Department of Transportation

December 2014

The contents of this report reflect the views of the authors who are responsible for the facts and the accuracy of the data presented herein. The contents do not necessarily reflect the official views or policies of the Georgia Department of Transportation or the Federal Highway Administration. This report does not constitute a standard, specification, or regulation.

1. Report No.: FHWA-GA-15-1315		2. Government Accession No.:		3. Recipient's Catalog No.:	
4. Title and Subtitle:  Assessment of Sand Quality on Concrete Performance: Examination of Acidic and Sulfate/Sulfide-Bearing Sands			5. Report Date: December 2014		
7. Author(s): Alvaro Paul, Kimberly E. Kurtis, Lawrence F. Kahn, Preet M. Singh			6. Performing Organization Code:		
9. Performing Organization Name and Address: Georgia Institute of Technology 790 Atlantic Drive, Atlanta, GA 30332			8. Performing Organ. Report No.:		
12. Sponsoring Agency Name and Address: Georgia Department of Transportation Office of Research 15 Kennedy Drive Forest Park, GA 30297-2534			10. Work Unit No.:		
			11. Contract or Grant No.: 0011717 (RP 1315)		
			13. Type of Report and Period Covered: Final; April 2013 – December 2014		
			14. Sponsoring Agency Code:		
15. Supplementary Notes:					
16. Abstract: The purpose of this research is to examine how the presence of sulfide- and sulfate-containing minerals in acidic aggregates may affect the properties of mortar and concrete. Analyses were performed to compare two sands from a deposit in the Georgia coastal area with a GDOT-approved natural sand. Results show that sulfide- and sulfate-bearing acidic sands present an important variability and could delay the hydration reactions of cement at early-age, could result in variability in the mechanical properties of concrete, and could accelerate the onset of delayed ettringite -induced expansion when subjected to a high temperature curing cycle. Also, these acidic sands may reduce the corrosion resistance of reinforced concrete. Based on these results, it is recommended that the use of this type of sand be avoided in prestressed concrete, precast operations, mass concrete, and other applications where an initial high temperature could be reached. It is also recommended that such sands be avoided in concrete structures exposed to marine environments. In other applications, if the sand source must be used, preliminary recommendations include the use of a sulfate-resistant Type V cement and use of appropriate supplementary cementitious materials (SCMs), although further evaluation of such material combinations is advised to ensure adequate performance.					
17. Key Words: acidic sands, sulfate, sulfide, corrosion, delayed ettringite formation, durability			18. Distribution Statement:		
19. Security Classification (of this report):  Unclassified	20. Security Classification (of this page):  Unclassified	21. Number of Pages:  92	22. Price:		



## TABLE OF CONTENTS

1. INTRODUCTION .....	1
1.1 Purpose of Research .....	1
1.2 Objectives .....	3
1.3 Organization of Report .....	4
2. LITERATURE REVIEW .....	6
2.1 Introduction .....	6
2.2 Sulfide Mineral Oxidation in Concrete .....	7
2.3 Low pH Conditions .....	9
2.4 Internal Sulfate Attack.....	11
2.5 Delayed Ettringite Formation .....	11
3. DESCRIPTION OF MATERIALS AND METHODS .....	16
3.1 Materials.....	16
3.1.1 Sands Sources Examined .....	16
3.1.2 Cement Composition.....	22
3.2 Mixture Designs for Mortar and Concrete .....	24
3.2.1 Mortar Mixtures .....	24
3.2.2 Concrete Mixture.....	25
3.3 Methods .....	26
3.3.1 Isothermal Calorimetry of Mortar Mixtures.....	26
3.3.2 Setting Times by Vicat Needle Method .....	27
3.3.3 Determination of Dynamic Elastic Modulus.....	28

3.3.4 Rapid Chloride Permeability Test (RCPT) .....	29
3.3.5 Accelerated Laboratory Method for Corrosion Testing of Reinforced Concrete Using Impressed Current (FM 5-522).....	30
3.3.6 Expansion of Mortar Bars due to ISA and DEF .....	33
4. EFFECT ON EARLY-AGE PROPERTIES.....	37
4.1 Setting Time by Vicat Needle Test.....	37
4.2 Isothermal Calorimetry.....	39
5. EFFECT ON MECHANICAL PROPERTIES OF CONCRETE.....	43
5.1 Compressive Strength Results .....	43
5.1 Dynamic Elastic Modulus Results.....	46
6. EFFECT ON DURABILITY .....	49
6.1 Rapid Chloride Penetration Test Results (RCPT) .....	49
6.2 Accelerated Corrosion Test .....	50
6.4 Potential for Internal Sulfate Attack (ISA).....	56
6.4 Potential for Delayed Ettringite Formation (DEF) .....	63
7. CONCLUSIONS AND RECOMMENDATIONS .....	76
7.1 Conclusions .....	76
7.2 Recommendations .....	78
7.3 Future Needs.....	79
REFERENCES .....	81
APPENDIX A: Modeled Degree of Hydration on Time.....	87
APPENDIX B: Individual Results of Compressive Strength of Concrete .....	89

APPENDIX C: Variability of Results - Accelerated Corrosion Testing ..... 92

## LIST OF TABLES

Table 1.1. Cement chemistry notation. ....	5
Table 3.1. Physical properties of sands.....	17
Table 3.2. Oxide analysis and Bogue potential composition of cements. ....	23
Table 3.3. Mortar mixture design for isothermal calorimetry test and setting time determination. ....	24
Table 3.4. Mortar mixture design for evaluation of potential for DEF and ISA. ....	24
Table 3.5. Concrete mixture design conforming GDOT Class AA1.....	25
Table 3.6. Slump and air content of fresh concrete. ....	26
Table 5.1. Statistical analysis of compressive strength results. Similarity of the results observed using acidic sands compared to control is tested.....	44
Table 5.2. Variability between Site H and Site D sand samples.....	45
Table 5.3. Dynamic elastic modulus at 28 and 90 days.....	47
Table 5.4. Statistical analysis of dynamic elastic modulus results. ....	47
Table 5.5. Estimations of the static modulus of elasticity from ACI 318 and BS 8110 equations. ....	48
Table 6.1. Total charge passed during RCPT performed at 56 days of age. ....	50
Table 6.2. Average resistance and time to failure of concrete samples for the corrosion test. ....	52
Table 6.3. Compressive strength of cubes at 28 and 100 days from mixing. ....	71
Table 6.4. EDS point analysis over regions A, B, and C of Figure 6.17. ....	75
Table B.1. Individual results of compressive strength test for control sand specimens. ..	89

Table B.2. Individual results of compressive strength test for Site H sand specimens. ... 90

Table B.3. Individual results of compressive strength test for Site D sand specimens. ... 91

## LIST OF FIGURES

Figure 2.1. Kelham curing cycle.....	15
Figure 3.1. Appearance of analyzed sands.....	16
Figure 3.2. Gradation curves of sands. Dashed lines show limits for fine aggregate according to ASTM C33. ....	17
Figure 3.3. pH variation over time. Initial pH of water was 6.95 for all the samples. ....	18
Figure 3.4. XRD pattern of the sands. Main peak at $2\theta = 26.67^\circ$ was truncated to highlight the differences between the sands. ....	19
Figure 3.5. XRD pattern of different sizes of Site H sand. Main peak at $2\theta = 26.67^\circ$ was truncated to highlight the differences between the samples. ....	20
Figure 3.6. Differential thermal analysis curves for control, Site H, and Site D sands. ...	21
Figure 3.7. Thermogravimetric curves for control, Site H, and Site D sands.....	21
Figure 3.8. TG curves for different particle sizes of Site H and Site D sands.....	22
Figure 3.9. Dynamic elastic modulus set up.....	29
Figure 3.10. RCPT set-up. Two specimens per mixture were tested at 56 days from casting. ....	30
Figure 3.11. Corrosion test samples with dimensions 4 in. diameter by 5.75 in. height. The exposed rebar was embedded to the mid-height of the cylinder. ....	31
Figure 3.12. High density polyethylene tanks for the corrosion test. A pump was used to maintain the concentration of the NaCl solution. ....	32

Figure 3.13. Specimens corresponding to each sand type were kept separately to avoid interaction during the test.....	33
Figure 3.14. Mortar bars for length change testing and mortar cubes for compressive strength evaluation over time.....	34
Figure 3.15. Metallic tray used to provide a moist condition during Kelham curing cycle. .....	35
Figure 3.16. Mortar samples were kept in a moist environment for the first 24 hours after casting. Aluminum foil was used to avoid water evaporation during Kelham curing cycle. .....	36
Figure 3.17. Compression frame used for strength assessment of mortar cubes.....	36
Figure 4.1. Initial and final setting times of mortars prepared using Cement A.....	38
Figure 4.2. Calorimetry results for mortar mixtures prepared with Cement A.....	39
Figure 4.3. Calorimetry results for mortar mixtures prepared with Cement B.....	40
Figure 4.4. Calorimetry results for mortar mixtures prepared with Cement C.....	41
Figure 4.5. Cumulative heat of hydration curves for the first 72 hours.....	42
Figure 5.1. Average compressive strength of concrete at 1, 3, 7, 28, 56, and 90 days after casting. Each point corresponds to the average of three cylinders and the error bars show the standard deviation. ....	44
Figure 6.1. Current over time for concrete samples exposed to a NaCl solution. Every line represents the average of three specimens. ....	51
Figure 6.2. Specimens for Control Sand at 0, 30, and 50 days from the start of the test..	53
Figure 6.3. Specimens for Site D Sand at 0, 30, and 50 days from the start of the test....	54
Figure 6.4. Specimens for Site H Sand at 0, 30, and 50 days from the start of the test....	55

Figure 6.5. Expansion of mortar bars due to ISA (Cement A). Error bars represent standard deviation. ....	58
Figure 6.6. Expansion of mortar bars due to ISA (Cement B). Error bars represent standard deviation. ....	59
Figure 6.7. Expansion of mortar bars due to ISA (Cement C). Error bars represent standard deviation. ....	60
Figure 6.8. Expansion of mortar bars due to ISA (Cement D). Error bars represent standard deviation. ....	61
Figure 6.9. Expansion of mortar bars due to ISA (Cement E). Error bars represent standard deviation. ....	62
Figure 6.10. Expansion of mortar bars due to DEF (Cement A). Error bars represent standard deviation. ....	65
Figure 6.11. Expansion of mortar bars due to DEF (Cement B). Error bars represent standard deviation. ....	66
Figure 6.12. Expansion of mortar bars due to DEF (Cement C). Error bars represent standard deviation. ....	67
Figure 6.13. Expansion of mortar bars due to DEF (Cement D). Error bars represent standard deviation. ....	68
Figure 6.14. Expansion of mortar bars due to DEF (Cement E). Error bars represent standard deviation. ....	69
Figure 6.15. Backscattered micrograph of a DEF-affected mortar sample (200 X).....	73
Figure 6.16. Backscattered micrograph of a DEF affected mortar sample (550 X). ....	74
Figure 6.17. Backscattered micrograph of a DEF affected mortar sample (1,400 X). ....	74

Figure A.1. Degree of hydration for mortars using Cement A. ....	87
Figure A.2. Degree of hydration for mortars using Cement B. ....	87
Figure A.3. Degree of hydration for mortars using Cement C. ....	88
Figure C.1. Evolution of current during the test for concrete specimens. ....	92
Figure C.2. Evolution of current during the test for control sand specimens. ....	92
Figure C.3. Evolution of current during the test for Site H sand specimens. ....	93
Figure C.4. Evolution of current during the test for Site D sand specimens. ....	93

## **EXECUTIVE SUMMARY**

The purpose of this research is to examine how the presence of sulfide- and sulfate-containing minerals in acidic aggregates may affect the properties of mortar and concrete. Analyses were performed to compare two sands from a deposit in the Georgia coastal area with a GDOT-approved natural sand.

Results show that sulfide- and sulfate-bearing acidic sands present an important variability and could delay the hydration reactions of cement at early-age, could result in variability in the mechanical properties of concrete, and could accelerate the onset of delayed ettringite-induced expansion when subjected to a high temperature curing cycle. Also, these acidic sands may reduce the corrosion resistance of reinforced concrete.

Based on these results, it is recommended that the use of this type of sand be avoided in prestressed concrete, precast operations, mass concrete, and other applications where an initial high temperature could be reached. It is also recommended that such sands be avoided in concrete structures exposed to marine environments. In other applications, if the sand source must be used, preliminary recommendations include use of a sulfate-resistant Type V cement and use of appropriate supplementary cementitious materials (SCMs), although further evaluation of such material combinations is advised to ensure adequate performance.

## **ACKNOWLEDGEMENTS**

The research presented in the following report was sponsored by the Georgia Department of Transportation through Research Project Number RP 13-15. The authors would like to acknowledge Scott Harris, Aggregate Geologist, for his assistance in acquiring the materials used for this project and providing information on the sands and their geological source. The support and guidance of Georgene Geary, State Research Engineer, and Peter Wu, Bureau Chief, is also greatly appreciated.

The authors would also like to acknowledge the assistance of undergraduate students Simon Reiter, Daniella Remolina, John Jung, Jaime Ghitelman, and PhD student Mehdi Rashidi in the mixing and testing of samples.

The opinions and conclusions expressed herein are those of the authors and do not represent the opinions, conclusions, policies, standards or specifications of the Georgia Department of Transportation or of other cooperating organizations.

# 1. INTRODUCTION

## 1.1 Purpose of Research

In late 2012, sand samples from a previously unexploited, unique geological source located in the Georgia Lower Coastal Plain were provided to Georgia Department of Transportation (GDOT), as a potential source of fine aggregate for use in cement-based materials. Tertiary and quaternary uppermost sediments from this area are composed mostly of pale to dark-green, phosphatic, very sandy micaceous clays which are interbedded with fine to coarse phosphatic sand [Herrick and Vorhis, 1963]. The sand deposit is located in the Pamlico geological formation, which corresponds to a lowland habitat, flanked by natural barrier systems, in Hinesville, GA [Hails and Hoyt, 1969]. The sand has been extracted from depths of 70 to 80 feet and corresponds to the Pliocene geological age (2.6 to 5.3 million years before present). Preliminary analysis performed by GDOT identified the presence of iron sulfide and noted the unusually low pH of the sands.

It is known that presence of sulfate- or sulfide-bearing<sup>1</sup> minerals in aggregates used in concrete can be problematic. While calcium sulfate dihydrate (or gypsum) is commonly added to portland cement to control the reaction of the tricalcium aluminate phase, for

---

<sup>1</sup> The chemical formula for the sulfate ion is  $\text{SO}_4^{2-}$ ; sulfide is  $\text{S}^{2-}$ ; for sulfite, which is more commonly found in salts (e.g., sodium sulfite,  $\text{Na}_2\text{SO}_3$ ), the formula is  $\text{SO}_3^{2-}$ .

any cementitious clinker and source of sulfate,<sup>2</sup> an optimal content or ratio of these components can be identified which produces appropriate setting characteristics and early strength development in concrete [Taylor, 1997]. As a result, additional sources of sulfate can affect time to set and strength development, particularly at early ages. At later ages, if sulfur-containing species derived from aggregates interact chemically with the surrounding hydrated cement paste, expansion and cracking and other forms of damage may result; this is “internal sulfate attack” as the source of the aggressive ion is within the concrete, rather than external (as in “sulfate attack”). Internal sulfate attack is most commonly observed in the Middle East (see for example Zein Al-Abidien [1987]). In cases of mass concrete construction, heat curing, or some hot weather construction where internal temperature of the concrete exceeds 165-170 °F (70-80 °C), damage by delayed ettringite formation (DEF) may also be problematic due to the potential increased availability of sulfates [Atahan and Dikme, 2010].

Further, oxidation of some such sulfide-bearing minerals can result in the production of sulfuric acid. Acids can substantially interfere with and potentially prevent setting of plastic concrete and can lead to significant degradation of hardened properties, largely because products of cement hydration are unstable at pH lower than 9-11. In reinforced concrete, if the pore solution pH is sufficiently lowered to depassivate the steel or if the sulfate ion concentration is sufficiently high to locally compromise the passive layer,

---

<sup>2</sup> In cement chemistry, oxide notation is used where ‘Sbar’ or  $\bar{S}$  denotes “sulfate” as  $SO_3$ .

corrosion can occur prematurely. Thus, the presence of sulfates ( $\bar{S}$ ) in sufficient amounts within the mineral phases comprising an aggregate source, as well as the associated production of acids, have the potential to negatively affect both the early age properties and long-term durability of concrete, but these potential effects have not been the subject of extensive prior published research.

At this time, neither GDOT specifications nor ASTM C33 Standard Specification for Concrete Aggregates provide limits on aggregate pH or sulfate or sulfide content in fine aggregate. However, for coarse aggregate used in concrete, GDOT Section 800 specifications do provide for a 0.01% limit on sulfur content for bridge type structures. Some international standards provide some limits on sulfate content, typically expressed either as  $\text{SO}_3$  content by percent mass of the aggregate or by percent mass of cement used in the concrete mix [Khedder and Assi, 2010].

In regions where sulfate-containing aggregates are more common, lower  $\text{SO}_3$  limits may be imposed on cements. For example, in Iraq, where sulfate-free aggregates are scarce,  $\text{SO}_3$  allowed in ordinary portland cement is limited to 2.8% which is considerably lower than British (3.5%) and ASTM specifications (3.0 %) for general use cements [Al-Rawi et al., 2002]. However, ASTM does limit  $\text{SO}_3$  more stringently for low heat of hydration or highly sulfate resistant cement (2.3%).

Aggregate pH or acidity does not appear to be addressed in existing standards.

## **1.2 Objectives**

The purpose of this investigation is to evaluate the performance of local sand sources, including those containing sulfide or sulfate minerals, as fine aggregate in concrete. The

combination of sulfide or sulfate-containing sand on (1) early age properties (i.e., setting time, early age strength), (2) strength development, and (3) durability will be compared to those of other accepted sand sources. Results from this investigation will be used to better understand the implications of pH and mineral content on short and long-term performance and to make recommendations for the use of such sources, including any necessary changes to GDOT concrete aggregate specifications.

### **1.3 Organization of Report**

This report is composed of seven chapters.

Chapter 2 presents a background review of the impact of the use of sulfate- and sulfide-bearing sands on the properties of cement-based materials.

Chapter 3 describes the characteristics of the analyzed sands and comprises the tests and methods performed during the project.

Chapters 4, 5, and 6, summarize the effect of the sands on early age properties, mechanical properties, and durability of concrete and mortar, which lead to conclusions and recommendations presented in Chapter 7.

Additionally, cement chemistry notation is used along the document. The shorthand notation for oxides present in cement-based materials is shown in Table 1.1.

**Table 1.1.** Cement chemistry notation.

Oxide	Short Notation
CaO	C
SiO <sub>2</sub>	S
Al <sub>2</sub> O <sub>3</sub>	A
Fe <sub>2</sub> O <sub>3</sub>	F
MgO	M
K <sub>2</sub> O	K
Na <sub>2</sub> O	N
SO <sub>3</sub>	$\bar{S}$
CO <sub>2</sub>	$\bar{C}$
H <sub>2</sub> O	H

## 2. LITERATURE REVIEW

### 2.1 Introduction

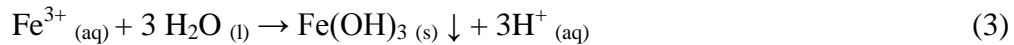
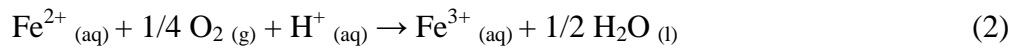
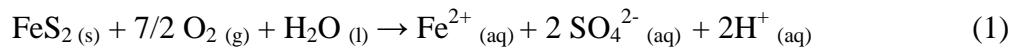
Sulfur represents a 0.07% of the constituents of Earth's crust [Brimblecombe, 2003], where it is found in gypsum and metal sulfides. Sulfur in the atmosphere is mostly contained in sulfur dioxide (SO<sub>2</sub>) and hydrogen sulfide (H<sub>2</sub>S) derived from volcanic activity, while in seawater, sulfur is found mainly as dissolved sulfate [Böttcher, 2011]. Microbial sulfate reduction is the most important process for the presence of iron sulfides in soils, and evaporitic sulfate materials like gypsum and dihydrate can be precipitated from seawater [Rickard and Luther, 2007; Böttcher, 2011].

Soils containing sulfidic materials, also known as acid sulfate soils, are present in marine environments, after formation of wetlands, lakes and disposal ponds by human activity, or due to saline groundwater discharge produced by vegetation clearing. Undisturbed sulfide minerals do not present acidification, which is triggered by exposure to oxygen in the air and occurs when the amount of acid produced overcomes the buffer capacity of the soil [Fitzpatrick et al., 2009].

The presence of sulfide and sulfate in aggregate sources, and their potential for low pH, could affect the properties of cement-based materials containing them. In this chapter, a review of the effects of the oxidation of iron sulfides, the occurrence of internal sulfate attack and delayed ettringite formation, and the effects of low pH conditions in concrete is presented.

## 2.2 Sulfide Mineral Oxidation in Concrete

Sulfide minerals are metal sulfide compounds that include chalcopyrite (CuFeS<sub>2</sub>), sphalerite (ZnS), molybdenite (MoS<sub>2</sub>), galena (PbS), cinnabar (HgS), and pyrite (FeS<sub>2</sub>). Pyrite is the most commonly found sulfide in geological environments. When sulfides are exposed to the air, they react with oxygen and water to release protons (H<sup>+</sup>). Overall, this reaction results in a decrease in pH. Equations 1 to 3 summarize this reaction for pyrite [Nordstrom, 2011].



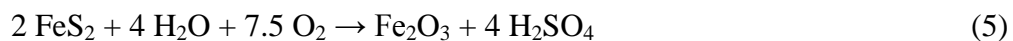
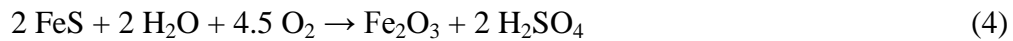
The oxidation of sulfide minerals depends on the mineral type (monosulfide or disulfide), solubility, defects, and surface area, as well as temperature and the presence of bacteria. Monosulfide (e.g., FeS and ZnS) reactivity increases with increasing solubility due to the reaction with acid to form H<sub>2</sub>S, which oxidizes to form sulfur and sulfate. Disulfides (e.g., FeS<sub>2</sub> and FeAsS) will not form H<sub>2</sub>S, but elemental sulfur and thiosulfate (S<sub>2</sub>O<sub>3</sub><sup>2-</sup>). Also, some sulfides, such as molybdenite, are fairly insoluble and undergo very slow oxidation. Finer particles will react and dissolve faster [Nordstrom and Southam, 1997; Nordstrom, 2011]. Additionally, several types of bacteria catalyze the oxidation reaction, reducing elemental sulfur into sulfuric acid [Hawkins, 2014].

In concrete, the presence of mineral sulfides as a minor constituent of aggregates can produce deleterious reactions. Two common mineral sulfides found in aggregate are

pyrite ( $\text{FeS}_2$ ) and pyrrhotite ( $\text{Fe}_{1-x}\text{S}$ , where  $x = 0-0.125$ ), a less ordered and consequently more reactive form of iron sulfide [Hawkins, 2014]. Pyrite and pyrrhotite can be present in igneous, metamorphic or sedimentary rocks, and usually develop in marine environments, inland wet regions, or close to faults. The formation of pyrite in sedimentary deposits is associated with the reaction of iron minerals with  $\text{H}_2\text{S}$ , generated by sulfate reduction under bacterial action, to produce metastable iron monosulfides, which transform into pyrite [Berner, 1984]. The availability of organic matter and dissolved sulfate control the rate of the reaction and the amount of pyrite formed. Marine conditions commonly provide suitable conditions for this reaction. In particular, in oxygen-depleted regions under the surface of marine sediments, higher concentrations of pyrite have been reported due to conditions which are favorable for the degradation of less reactive iron minerals by  $\text{H}_2\text{S}$  [Berner, 1984].

Pyrite and pyrrhotite oxidize in presence of water and oxygen, a process which starts in the first minutes of exposure [Chandra and Gerson, 2010] and over time develops acidic by-products rich in iron and sulfate [Rodrigues et al, 2012]. The oxidation of iron sulfides may be accelerated in conditions of higher alkalinity, such as the high pH environment provided by cement paste in mortar and concrete mixtures.

These reactions can be summarized by [Schmidt et al, 2011]:



Two evident effects of the oxidation reaction could be noted. One is the volume increase resulting from the oxidization of iron sulfides, with the volume of the products around 1.3 to 1.7 times those of the reactants. Depending on the degree of reaction, the expansion will generate stresses. If the expansion overcomes the strain limit of the aggregates or surrounding cementitious material, it will lead to cracking [Schmidt et al, 2011]. A second effect is the generation of sulfuric acid ( $H_2SO_4$ ), that decreases pH upon contact with water, followed by a more gradual decrease until a stable value is reached, generally after several days [Chinchon and Aguado, 2012]. The pH reduction of pyrite is greater than pyrrhotite, producing a final value of 3 compared to 4.5, while pyrrhotite's supply of sulfate and ferrous ions is higher than the case of pyrite. The implications of a pH reduction on the local or global properties of concrete containing such aggregate are not clear, but it is well known that products of portland cement hydration are unstable at pH below 9-11, depending upon the phase [Glasser, 2002].

In addition, also in portland cement-based materials, an indirect effect of the oxidation of iron sulfides and the consequent release of sulfate ions is the potential formation of late ettringite and also gypsum. Durability could be compromised due to internal sulfate attack (ISA) and/or delayed ettringite formation (DEF) in such cases.

### **2.3 Low pH Conditions**

The exposure of concrete to acidic conditions can adversely affect its performance. This can include loss of strength and adhesion in the paste, and as a result, loss of strength and increased permeability in the concrete. Also, earlier initiation of

corrosion and a subsequently accelerated rate of corrosion of steel reinforcement is possible.

In good quality concrete, steel embedded in concrete is exposed to an alkaline environment ( $\text{pH} > 11$ ), developing a thin (1-10 nm), highly protective and insoluble passive film, which provides considerable corrosion resistance to the steel [Jones, 1996]. A reduction of the pH makes this passive layer thermodynamically unstable and a faster dissolution of steel will be induced [Hansson, 1984]. In the case of prestressed concrete, the acidification of the crevice region, space left by the prestressing wires with oxygen deficiency, leads to an earlier corrosion initiation compared to reinforced concrete and to a reduced chloride threshold limit (CTL) compared to an isolated prestressing wire [Moser et al., 2011].

Additionally, exposure to acid – or any pH lower than the high pH common in portland cement-based systems – can compromise the stability of the hydrated phases, which act to bind the aggregate together, providing strength and impermeability. When concrete is exposed to an acidic environment (e.g., in sewer pipes, wastewater treatment plants, or cooling towers), the reduction of the pH of the pore solution will induce the selective decomposition of hydration products: calcium hydroxide at pH below 12.6, ettringite at pH below 10.7, and C-S-H at pH below  $\sim 10.5$  [Beddoe and Dorner, 2005]. The loss of these cement hydrates will decrease adhesion, compromising mechanical properties and increasing permeability.

In the case of sulfuric acid attack, the effects of acid attack can be combined with those of sulfate attack. That is, calcium hydroxide will react with sulfate to form gypsum

[Monteny et al., 2000]. The formation of other sulfate-bearing phases may also be possible, depending upon the pH.

#### **2.4 Internal Sulfate Attack**

Internal sulfate attack (ISA) is a particular case of sulfate attack where the sources of sulfate come from one or more constituent materials, commonly from cementitious materials or contaminated aggregates. ISA could occur due to the presence of sulfate-bearing aggregates or over-sulfation of the cement. In these cases, a  $\text{SO}_3$  content greater than 5 or 6% by weight of cement is generally believed to be necessary to generate expansion [Scrivener and Skalny, 2005].

Products of internal sulfate attack include gypsum (calcium sulfate dihydrate) and ettringite. In the presence of magnesium, the formation of brucite, among other products, is possible [Neville, 2004]. The later formation of ettringite, in particular, is sometimes associated with deleterious expansion, which can compromise mechanical properties and increase permeability. The formation of gypsum is also associated with a decrease in strength, loss of adhesion and potential decrease in pore solution pH. Overall, ISA can compromise the strength and integrity of the affected concrete, leading to a decrease in service life.

#### **2.5 Delayed Ettringite Formation**

DEF can lead to expansion, cracking, and loss of mechanical properties and durability of concrete. This damage is commonly attributed to the formation of ettringite after concrete hardens [Taylor et al., 2001], and it has been associated with concrete

which has experienced exposure to temperatures exceeding 65-70 °C. DEF has been noted to produce damage in precast concrete, where steam and higher temperature curing are used, and in mass concrete elements, where the heat evolution from cement hydration can lead to high internal temperatures [Thomas et al., 2006; Thomas and Ramlochan, 2004].

Ettringite ( $C_6A\bar{S}_3H_{32}$ ) is a product of ordinary portland cement hydration. It is first formed during the hydration of tricalcium aluminate ( $C_3A$ ), when  $C_3A$  reacts with gypsum ( $C\bar{S}\cdot H_2$ ) and water. As the sulfate availability decreases during early hydration (which is the common case in most cements), ettringite is considered as a metastable phase, decomposing into calcium monosulfoaluminate hydrate or “monosulfate” ( $3C_4A\bar{S}H_{12}$ ), a phase that contains less sulfate and binds less water than ettringite [Mindess et al., 2003].

While the mechanisms for damage by DEF remain the subject of continued study, it is believed that in ordinary portland cement (OPC) systems when internal temperatures exceed 65-70 °C, subsequently, in presence of moisture, the release of sulfate and aluminate ions from C-S-H are understood to combine with monosulfate to form late ettringite in confined spaces, which can produce expansion [Taylor et al., 2001; Ekelu et al., 2006; Flatt and Scherer, 2008]. With high temperatures during initial curing, ettringite is not a stable phase and decomposes, even at early ages. As a result, the aluminate and sulfate ions released are bound to the complex structure of the primary product of portland cement hydration, the calcium silicate hydrate or “C-S-H”. Here, aluminum can be substituted for silicon or can occupy interlayer spaces in C-S-H, where sulfates can also be loosely bound [Taylor et al., 2001]. After cooling, ettringite can form by

dissolution and precipitation, a reaction that consumes the sulfate present in monosulfate, pore solution and C-S-H, alumina from monosulfate, calcium from monosulfate and C-S-H, and water. In addition, a later decrease in the pore solution pH (such during consumption of hydroxyls and alkalis during the formation of alkali silica reaction gel), can also spur the release of aluminates and sulfates from C-S-H, leading to DEF.

Ettringite stability also depends on the pH of the pore solution and the availability of reactants. At pH levels lower than 11.5-12, ettringite can decompose to form hydrates of aluminum and/or gypsum [Santhanam et al., 2001], while when the pH is high ( $> 13$ ), the formation of monosulfate is favored [Taylor et al., 2001]. Similarly, Taylor et al. [2001] show that cements with  $\text{SO}_3$  content above 3% and  $\text{Al}_2\text{O}_3$  content above 4% could generate ettringite after cooling, suggesting the existence of one or more “pessimum”  $\text{SO}_3/\text{Al}_2\text{O}_3$  ratios.

The way this late formed ettringite produces expansion remains a subject of ongoing examination, but it is mostly accepted that i) an initial curing at a temperature above  $65^\circ\text{C}$  is needed for DEF to occur, ii) the cement or binder chemistry determines the amount of ettringite, and iii) the stresses developed depend on the microstructure of mortar or concrete [Taylor et al., 2001].

Currently, no standard test has been adopted by ASTM or AASHTO to assess materials, material combinations, or curing practices for the occurrence of DEF in portland cement concrete. But, common methods are used in practice, mostly involving mortar bar specimens exposed to an initial hot curing cycle, followed by immersion in limewater at standard room temperature. The mortar bar's length is monitored over time, and its expansion over time is calculated.

Two commonly used curing regimes for examining the potential for DEF are the Kelham and Fu methods. While the Kelham method generally produces higher expansions, earlier expansions are obtained by the Fu method [Folliard et al., 2006]. It should be noted that no expansion limit has been defined for a deleterious expansion due to DEF, but regularly 0.1% is considered an acceptable reference for mortars [Petrov and Tagnit-Hamou, 2004; Pavoine et al., 2012; Tovar-Rodríguez et al., 2013].

In this effort, the Kelham method was used to assess the potential for DEF when the various sands were combined with cements of varying composition. The Kelham method was selected because it involves a hot curing cycle and not an additional drying cycle as the Fu method. Details of the temperature-time variation in the Kelham curing cycle are shown in Fig. 2.1. The Kelham method [Kelham, 1997], increasingly used in recent research, resembles the heating regime of a precast concrete operation (see Fig. 2.1) and also addresses initial heat generation and accumulation during mass concrete placements.

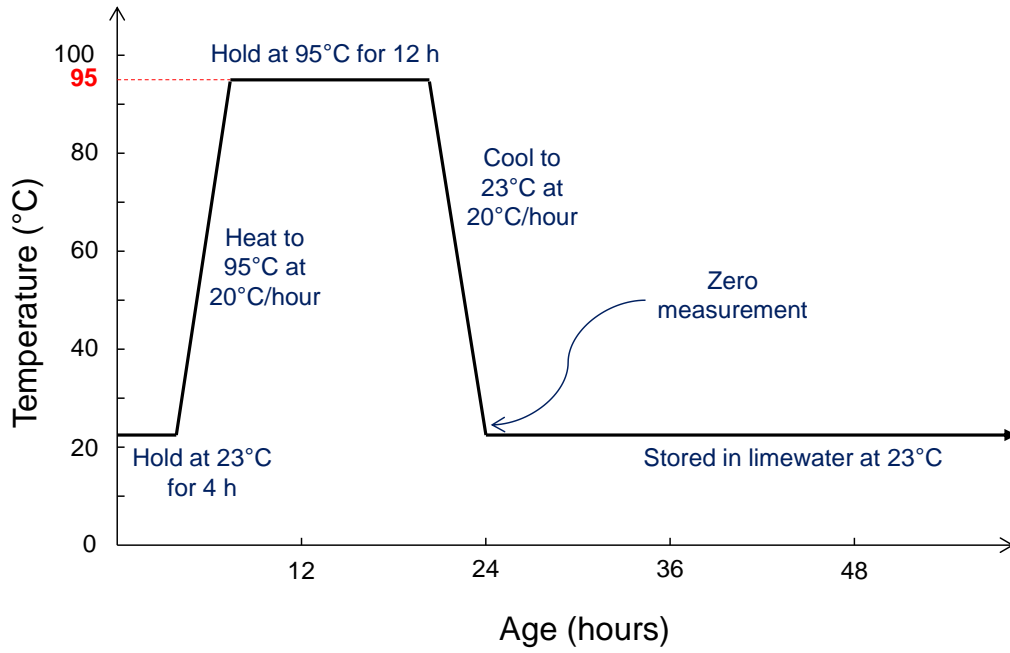


**Figure 2.1.** Kelham curing cycle.

### 3. DESCRIPTION OF MATERIALS AND METHODS

#### 3.1 Materials.

##### 3.1.1 Sands Sources Examined

In this effort, three different sands were considered. These include samples from two different stockpiles from the production facility in Hinesville, Georgia. These are denoted as Sites H and D. These were compared with a GDOT-approved natural sand obtained from Ridgecrest, Georgia (Figure 3.1). Throughout this report, the sands will be referred using these denominations: control, Site H, and Site D sands.

According to the producer, Site H sand has a water soluble sulfate ( $\text{SO}_4^{2-}$ ) content of 0.037% and a pyritic sulfur content of 0.020%, while Site D sand has a negligible amount of pyrite and 0.029% of water soluble sulfate content. The control sand has insignificant amounts of sulfate and pyritic sulfur.



**Figure 3.1.** Appearance of analyzed sands.

The aggregate gradation (see Figure 3.2) was measured using sieve analysis (AASHTO T27, technically equivalent to ASTM C136), while the specific gravities (SG) and absorption were obtained according to ASTM C127 and C128 (Table 3.1). The physical properties are similar for all the sands, and they served as input for the mortar and concrete mixture designs.

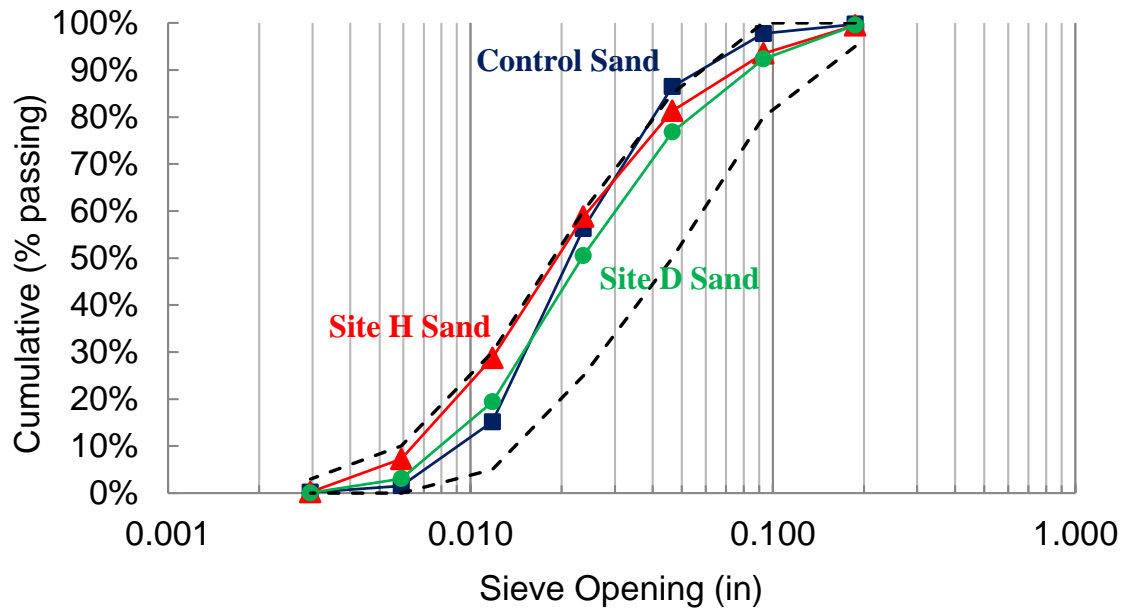


**Figure 3.2.** Gradation curves of sands. Dashed lines show limits for fine aggregate according to ASTM C33.

**Table 3.1.** Physical properties of sands.

	<b>Apparent SG (Dry)</b>	<b>SG Oven Dry</b>	<b>SG Saturated Surface Dry</b>	<b>Absorption</b>	<b>Fineness Modulus</b>
Control Sand	2.66	2.63	2.64	0.32%	2.43
Site H Sand	2.61	2.59	2.60	0.27%	2.31
Site D Sand	2.62	2.60	2.61	0.19%	2.58

To assess variations in pH among the sands, 250 g oven-dried samples of each of the sands were immersed in 300 mL tap water (pH = 6.95) in sealed containers, at 23 °C. The first measurement, which was made 30 minutes after the water was mixed with the sand, showed an abrupt drop of pH in the case of Site D and Site H sands, followed by small variations afterwards. The evolution of pH during 91 days can be observed in Figure 3.3. The control sand exhibits a near-neutral pH of just under 7, while the pH for Site D and Site H are acidic, exhibiting values of ~3 or less.

The variation in pH over time is consistent with the pH values associated with the oxidation of pyrite observed by Chinchon and Aguado [2012] using the same test. Also, the curve indicates an ongoing reaction that could be explained by the autocatalytic nature of pyrite oxidation in presence of acidophilic bacteria. However, pyrite was identified by the producer only for the Site H sand, not in Site D, while both sands showed similarly low pH values in water.

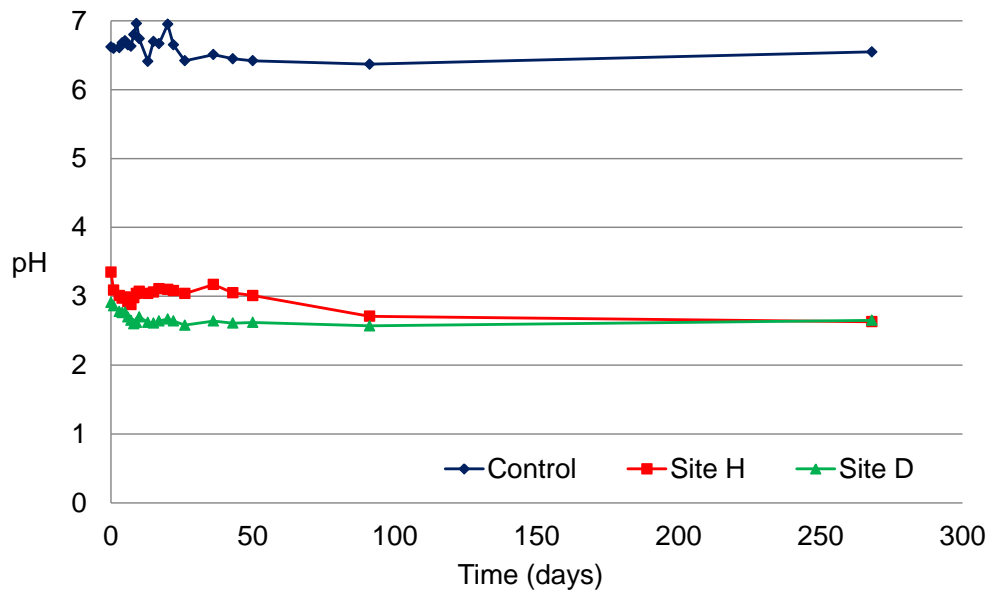


**Figure 3.3.** pH variation over time. Initial pH of water was 6.95 for all the samples.

To identify crystalline phases in each sand source, powder XRD diffraction was performed on a PANalytical X'Pert Materials Research Diffractometer equipped with a Cu-K $\alpha$  X-ray source. The XRD patterns (see Figure 3.4) show that the sands are composed mostly by quartz (identified with a *Q* in Figure 3.4), while Site H and Site D sands present additional peaks that can be attributed to alkali or plagioclase feldspar.

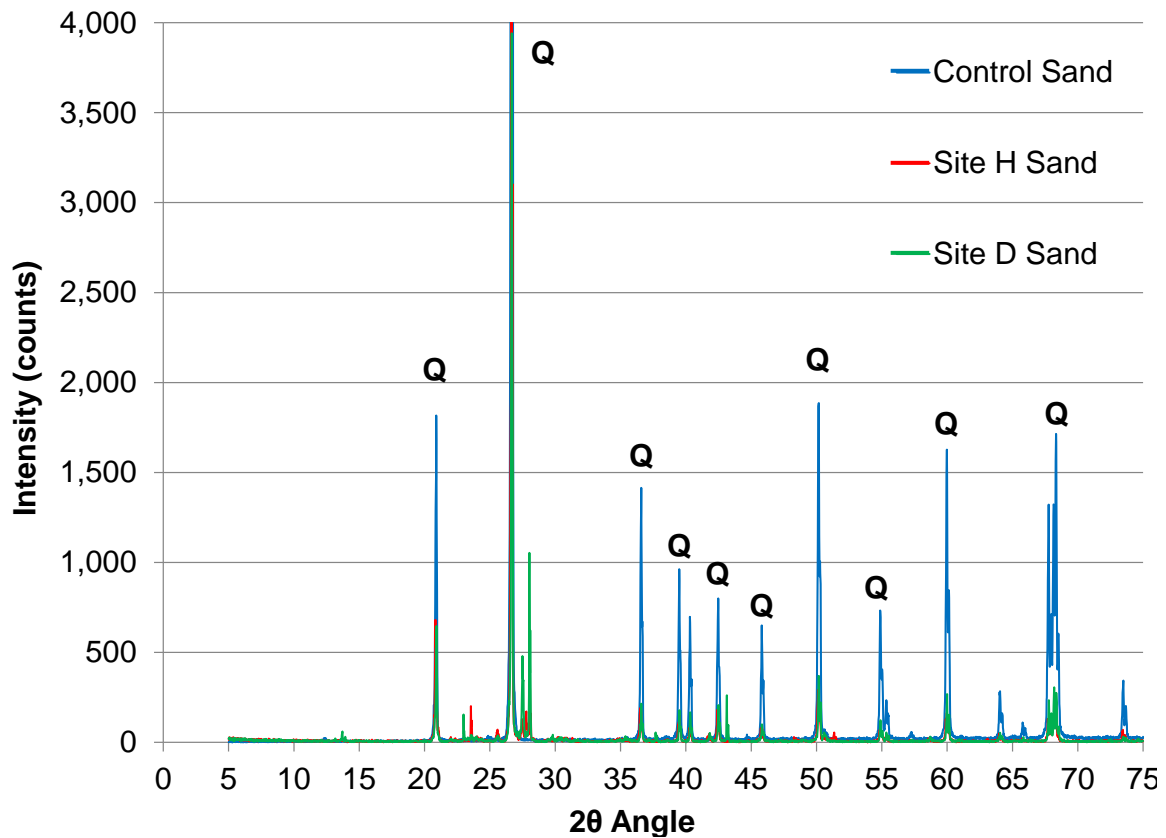


**Figure 3.4.** XRD pattern of the sands. Main peak at  $2\theta = 26.67^\circ$  was truncated to highlight the differences between the sands.

Sieved fractions of Site H sand were also analyzed by XRD. Patterns in Figure 3.5 show that there are differences in composition among the different fractions from Site H sand. The smallest particle sizes (finer than 38  $\mu\text{m}$ ) show the greatest variation from the bulk and show additional peaks that may be attributed to alkali or plagioclase feldspar.

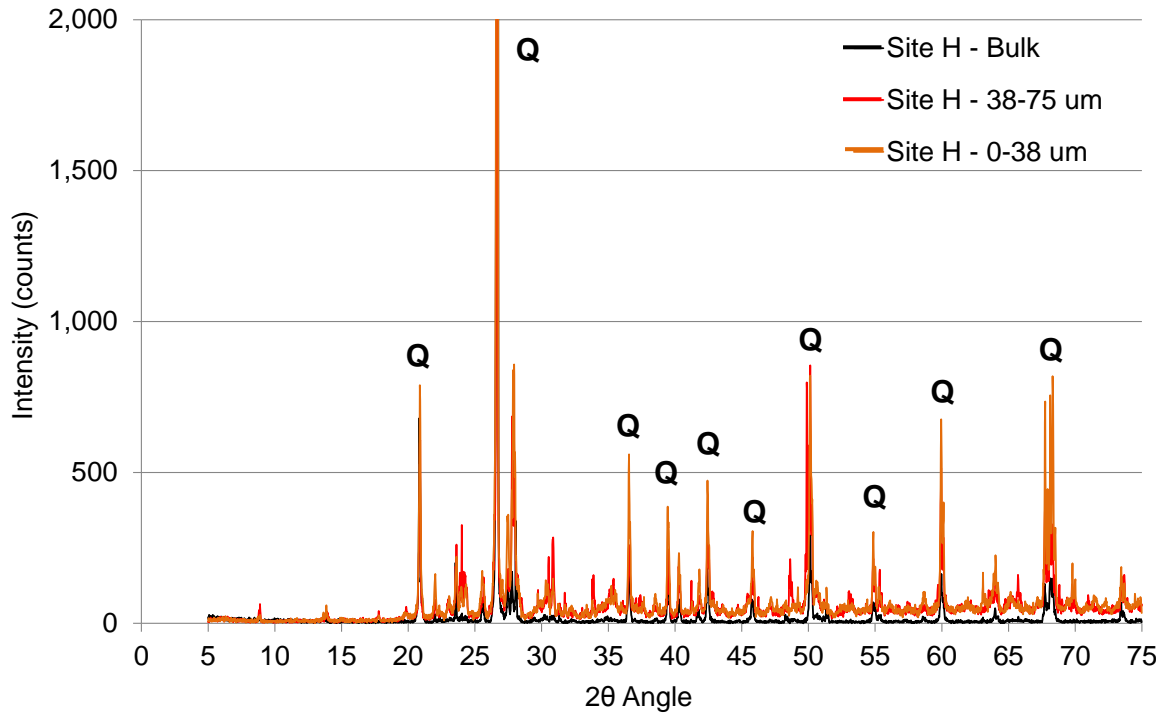


**Figure 3.5.** XRD pattern of different sizes of Site H sand. Main peak at  $2\theta = 26.67^\circ$  was truncated to highlight the differences between the samples.

The characterization of the sands was complemented by thermogravimetric analysis (TGA) combined with differential thermal analysis (DTA). DTA curves (Figure 3.6), normalized by ignited mass at every temperature, show the familiar phase transition of quartz, around 573  $^\circ\text{C}$ , from  $\alpha$ -quartz to  $\beta$ -quartz [Tsuneyuki et al., 1990]. DTA curves are similar for all the sands, but TG curves (Figure 3.7) show a more pronounced mass loss around phase transition temperature for control sand, and further mass decrease after

this point for acidic sands. This mass decrease at higher temperatures is more pronounced in the case of the smaller particle sizes of Site D and Site H sand (Figure 3.8), demonstrating along with the diffraction results that the composition of these sands varies with particle size.

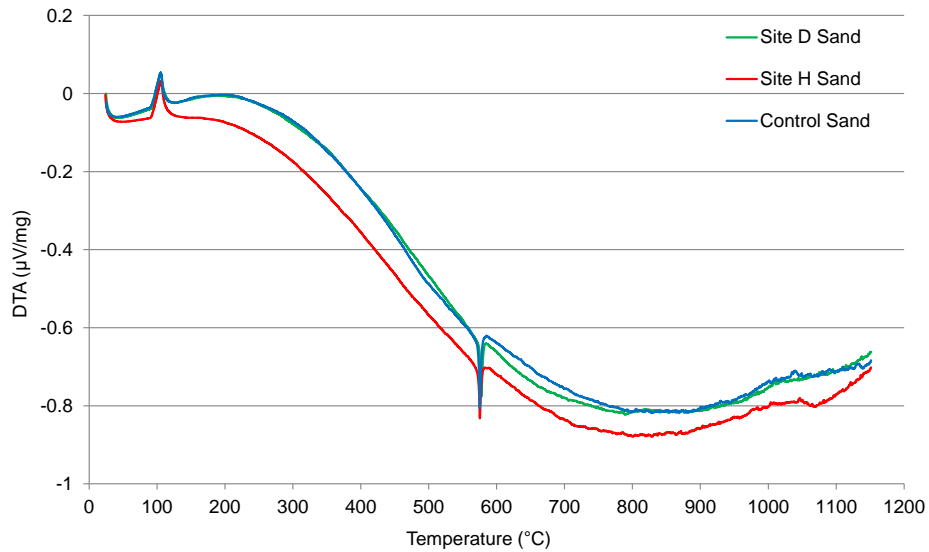


**Figure 3.6.** Differential thermal analysis curves for control, Site H, and Site D sands.

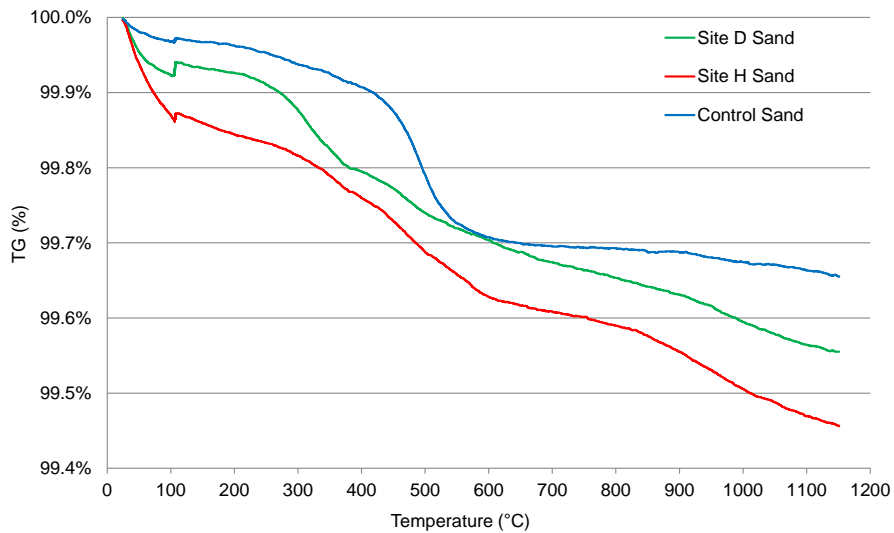


**Figure 3.7.** Thermogravimetric curves for control, Site H, and Site D sands.

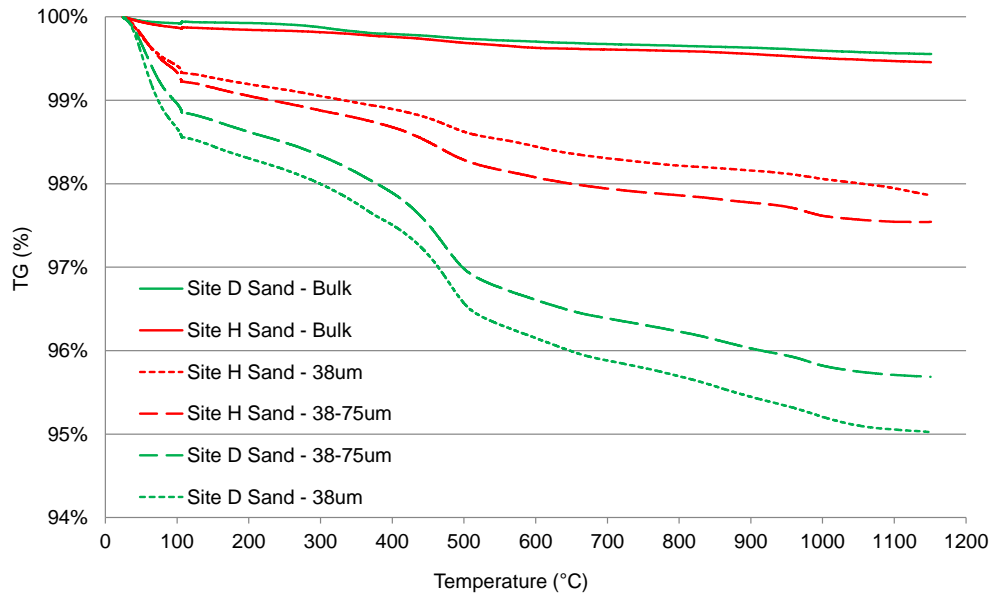


**Figure 3.8.** TG curves for different particle sizes of Site H and Site D sands.

### 3.1.2 Cement Composition

In total, five cements (labeled A through E) have been included in this investigation. Three cements (A, B, and C, see Table 3.2) have been used for the evaluation of the mechanical properties and durability assessment, while two additional cements (D and E, see Table 3.2) were included later and consequently partial results are included in this report. A range in cement composition was selected in order to understand interactions between cement and sand sources which may influence performance, including the occurrence and characteristics of a DEF reaction. According to previous research [Kelham, 1996; Taylor et al., 2001; Pavoine et al., 2012], ASTM C150 cement type, cement fineness,  $C_3A$  content, alkali content,  $SO_3$  content, and sulfate-to-alumina ratio ( $SO_3/Al_2O_3$ ), each may influence the potential for DEF. Because cement in Georgia tends to have lower alkali contents, high-alkali cement was not considered, with all the cements examined having a  $(Na_2O)_{eq}$  lower than 0.6%.

**Table 3.2.** Oxide analysis and Bogue potential composition of cements.

	<b>Cement A</b>	<b>Cement B</b>	<b>Cement C</b>	<b>Cement D</b>	<b>Cement E</b>
ASTM C150 Type	I/II	V	I/II	III	I
Blaine Fineness, m <sup>2</sup> /kg	393	376	413	498	401
SiO <sub>2</sub>	19.78%	21.10%	19.58%	19.81%	19.40%
Al <sub>2</sub> O <sub>3</sub>	4.61%	3.95%	4.79%	5.52%	5.48%
Fe <sub>2</sub> O <sub>3</sub>	3.37%	4.42%	3.38%	3.31%	3.33%
CaO	62.75%	62.49%	64.20%	63.99%	63.83%
MgO	3.07%	3.05%	1.06%	0.79%	0.79%
Na <sub>2</sub> O	0.13%	0.08%	0.19%	0.11%	0.12%
K <sub>2</sub> O	0.53%	0.55%	0.45%	0.55%	0.63%
(Na <sub>2</sub> O) <sub>eq</sub>	0.49%	0.44%	0.49%	0.47%	0.53%
TiO <sub>2</sub>	0.25%	0.24%	0.25%	0.33%	0.33%
Mn <sub>2</sub> O <sub>3</sub>	0.18%	0.22%	0.02%	0.04%	0.04%
P <sub>2</sub> O <sub>5</sub>	0.07%	0.10%	0.12%	0.23%	0.23%
SrO	0.08%	0.06%	0.05%	0.20%	0.20%
BaO	0.06%	0.06%	0.06%	0.06%	0.06%
SO <sub>3</sub>	2.55%	2.35%	3.26%	4.14%	3.18%
LOI	2.57%	1.33%	2.61%	1.67%	1.64%
<b>C<sub>3</sub>S</b>	62.08%	54.50%	66.26%	56.34%	61.76%
<b>C<sub>3</sub>A</b>	6.50%	2.97%	6.97%	9.03%	8.88%
<b>C<sub>2</sub>S</b>	9.89%	19.38%	6.15%	14.29%	9.03%
<b>C<sub>4</sub>AF</b>	10.26%	13.45%	10.28%	10.06%	10.14%
<b>SO<sub>3</sub>/Al<sub>2</sub>O<sub>3</sub> (mass ratio)</b>	0.55	0.59	0.68	0.75	0.58
<b>SO<sub>3</sub>/Al<sub>2</sub>O<sub>3</sub> (molar ratio)</b>	0.7	0.8	0.9	1.0	0.7

## 3.2 Mixture Designs for Mortar and Concrete

### 3.2.1 Mortar Mixtures

To examine early-age properties, isothermal calorimetry and Vicat setting time tests were performed on mortars produced with the mixture shown in Table 3.3. The water-to-cement ratio (w/c) and sand-to-cement ratio were 0.50 and 1.37, respectively, for all the mixtures. Cement A was used for setting time determination, and Cements A, B, and C were used for isothermal calorimetry testing.

**Table 3.3.** Mortar mixture design for isothermal calorimetry test and setting time determination.

<b>Constituent</b>	<b>Mixture Design, lbs/yd<sup>3</sup></b>
Cement	1,264
Water	634
Fine Aggregate (SSD)	1,733

Cements A to E were used to prepare the mortar bars and cubes. For the mortar cubes and bars, the sand-to-cement ratio in the mortar mixture was 2.75, as required in ASTM C109. The w/c for the mortar cubes and bars was kept at 0.50. The occurrence of DEF or ISA was assessed using this mixture design (see Table 3.4). Also, the mixing procedure followed ASTM C305.

**Table 3.4.** Mortar mixture design for evaluation of potential for DEF and ISA.

<b>Constituent</b>	<b>Mixture Design, lbs/yd<sup>3</sup></b>
Cement	882

Water	445
Fine Aggregate (SSD)	2,422

### 3.2.2 Concrete Mixture

The concrete mixture composition was determined in agreement with GDOT, conforming to class AA1 of the GDOT Specification 500: Concrete Structures. The w/c was 0.43 and air entrainment admixture was included in order to achieve 3-4% air by volume of concrete. This mixture design, using Cement A, was used to prepare cylindrical specimens for compressive strength, dynamic elastic modulus, rapid chloride permeability, and accelerated corrosion tests.

**Table 3.5.** Concrete mixture design conforming GDOT Class AA1.

<b>Constituent</b>	<b>Mixture Design, lbs/yd<sup>3</sup></b>
Cement	675
Water	291
Coarse Aggregate (SSD)	1,838
Fine Aggregate (SSD)	1,127
AE admixture (MB AE90)	0.7 oz./cwt

Additionally, the slump was determined using standard ASTM C143, and the air content of fresh concrete was obtained using the air meter Type B and the procedure described in standard ASTM C231. The results for these properties can be observed in Table 3.6. Differences were observed between the Site D and Site H sand concrete, with Site H exhibiting lower slump and lower air content than both the Site D sand and the

control. The underlying source of these variations is not clear, but it could be related to the greater fineness of this sand (see Figure 3.2 and Table 3.1) or its composition.

Concrete cylinders for mechanical properties determination were cast in 4" × 8" molds, covered with a plastic lid and demolded after 24 hours. Then, they were labeled and cured in a fogroom until the age of testing.

**Table 3.6.** Slump and air content of fresh concrete.

	<b>Slump, in</b>	<b>Air content, %</b>
Control Sand	1.5	3.5
Site H Sand	0.5	2.5
Site D Sand	2.0	3.5

### **3.3 Methods**

#### **3.3.1 Isothermal Calorimetry of Mortar Mixtures**

To evaluate the effect of the acidic sands on the hydration kinetics of cements with variable cement composition (see Table 3.2), isothermal calorimetry was performed at 25 °C in an 8-channel TAM AIR microcalorimeter, with a precision of  $\pm 2 \mu\text{W}$  and accuracy greater than 95%, according to standard ASTM C1679. Pastes were prepared from each cement with deionized water with a hand-held mixer, following procedures in ASTM C1679.

Eight samples were prepared for every cement, three per each acidic sand and two for control. The reason for the use of an additional sample for the acidic sands is the concern for their variability. In every case, the ampules were filled with  $15 \pm 1$  g of mortar, recording the weight with a precision of 0.01 g. All the replicates of the same

mixture were introduced into the calorimeter within a minute of one another, to limit interactions with the rest of the samples. Also, the time of initial contact between cement and water, and the time where the ampules were loaded into the calorimeter were recorded. The power of every ampule was recorded in mW every 60 s and later normalized by mass of cement. Data were collected for at least three days for every cement (i.e., Cements A-E).

### 3.3.2 Setting Times by Vicat Needle Method

Setting time of mortars prepared with Cement A were measured by ASTM C191. The same mixture composition used for isothermal calorimetry was considered for this test (see Table 3.3). This method considers the use of the Vicat apparatus, a metallic base where the tested specimen is placed under a needle that is released from a fixed position. The depth of penetration or mark on the surface of the specimen is monitored in time in order to obtain the initial and final setting times.

The specimen consisted of a mortar sample cast in a conical ring with a height of 40 mm. Two specimens were prepared per mixture. Between measurements, the specimens were kept in sealed containers at high relative humidity (RH) to avoid drying.

The penetration of the needle is monitored until a value of 25 mm or less is obtained. The time between the initial contact of cement and water and time when 25 mm of penetration is observed is considered the initial setting time by the standard. When the needle does not leave a mark on the surface of the specimen, the test is concluded and the final setting time is recorded.

### 3.3.3 Determination of Dynamic Elastic Modulus

Along with the compressive strength test, the dynamic elastic modulus was measured at 28 and 90 days, on 4" x 8" cylinders, according to ASTM C215. Three cylinders per mixture were measured at each age of testing. Using the impact resonance method, the fundamental resonant frequency was obtained. In this non-destructive test, the cylinder is placed on a steel support that allows the cylinder to vibrate freely after a strike is applied by an impactor at the center of the end surface. An accelerometer triggers data acquisition and a waveform analyzer records the resonant longitudinal frequency (see Figure 3.9). This value was used to calculate the dynamic elastic modulus (Equation 6).

$$\text{Dynamic } E = DM(n')^2 \quad (6)$$

where  $M$  is the mass of the concrete specimen, in kg,  $n'$  is the fundamental longitudinal frequency, in Hz, and  $D$  is calculated from  $5.093(L/d^2)$ , with  $L$ , the length of the cylinder, in meters, and  $d$ , the diameter of the cylinder, in meters. Three replicate cylinders were tested for each mixture and age of testing. It should be noted that the dynamic  $E$  obtained by ASTM C215 is higher than the static  $E$  obtained by ASTM C469. Depending on the equation used to relate both mechanical properties, the difference ranges between 20 and 30%.



**Figure 3.9.** Dynamic elastic modulus set up.

#### 3.3.4 Rapid Chloride Permeability Test (RCPT)

The RCP test (Figure 3.10) was performed on 2-in sections of 4" x 8" cylinders obtained after 56 days of fogroom curing. Concrete was prepared using the mixture design in Table 3.5. Three replicate specimens were tested per analyzed sand, following the procedure in ASTM C1202. These sections were saturated at vacuum pressure in water for three hours, and soaked under water for 18 hours. Then, cells were mounted at the ends of the specimen. One cell contains a 3% NaCl solution and the other contains a 0.3N NaOH solution, with both solutions accessible to the concrete specimen. The test was initiated when electrical connections were attached to impose a voltage of 60 V during 6 hours, and the charge that passed along the specimen was recorded. According to ASTM C1202, chloride penetrability can be assessed according to the total charge at the end of the test.



**Figure 3.10.** RCPT set-up. Two specimens per mixture were tested at 56 days from casting.

### 3.3.5 Accelerated Laboratory Method for Corrosion Testing of Reinforced Concrete Using Impressed Current (FM 5-522)

The accelerated test Florida Method (FM) 5-522 (Florida DOT, 2000) was performed to evaluate the effect of the analyzed sands on the corrosion behavior of reinforced concrete. This test can be used to compare the time to corrosion among different concrete mixtures. This test was selected in consultation with GDOT and the sand producer as a means to assess the influence of the sand source on the potential for corrosion in concrete. The test provides relatively rapid results compared to other standardized test methods for corrosion.

The concrete specimens for this test were prepared using the same mix design exposed above (see Table 3.5), using Cement A (Type I/II cement), with the addition of superplasticizer (Glenium 3030NS) at 3 oz/cwt. The specimens had dimensions 4 in. diameter by 5.75 in. height and a #4 reinforcing bar embedded through the mid-length of

each cylinder (Figure 3.11). The steel bars were preconditioned through a bath of sulfuric acid solution and mechanical brushing that removed the iron oxide of the surface, per standard specifications.



**Figure 3.11.** Corrosion test samples with dimensions 4 in. diameter by 5.75 in. height. The exposed rebar was embedded to the mid-height of the cylinder.

After demolding, the specimens were cured 28 days in a fogroom and were subsequently immersed in a 5% NaCl solution for additional 28 days, as described in the test procedure. The bars were not protected during the curing process or during immersion, but the condition of the steel surface was evaluated and no evidence of corrosion was observed. After this period, the specimens were stored in open polyethylene containers, submerged partially in a 5% NaCl solution, with the solution waterline at 3 to 4 inches from the bottom of the tank (Figure 3.12), depth that was controlled during the execution of the test. 5% NaCl solution was circulated in the test container using an external pump. Also, the top section of the rebar was sandblasted to assure the electrical connection. An additional rebar was also immersed in the solution

(Figure 3.13) as a counter electrode for the impressed current to maintain the applied voltage. Then, a voltage of 6 V was applied between the concrete-embedded bars and the counter electrode, a step that represented the time zero measurement. To measure the current flow of the circuits, 0.1  $\Omega$  electrical shunts were placed in every circuit. Potential drop across this shunt was recorded and used to measure the current throughout these tests. Additionally, the applied voltage was measured at different points to control the applied potential value required by FM 5-522. Three specimens for each type of sand were tested and the formation of surface cracks in concrete and corrosion products was constantly monitored.

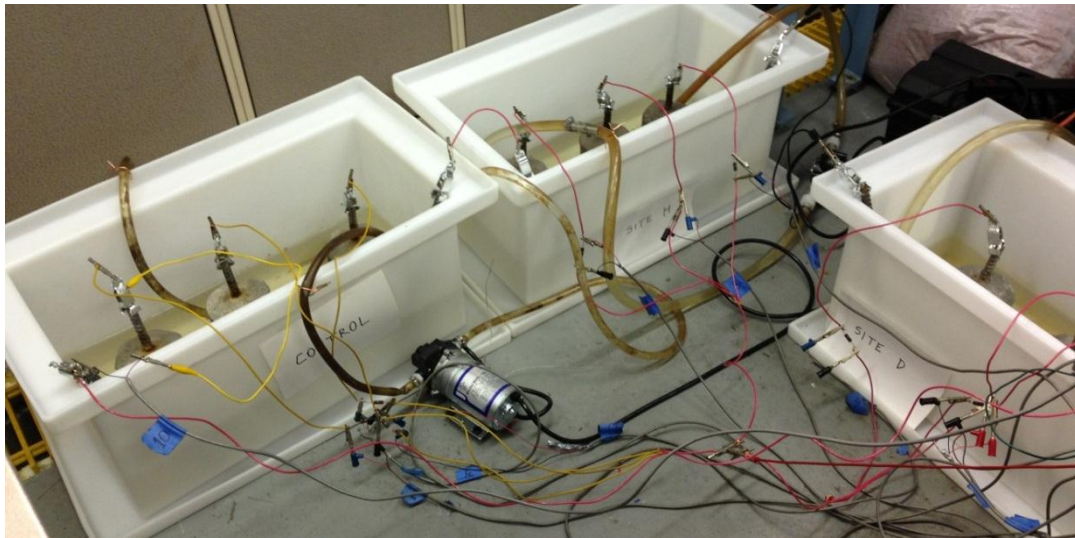


**Figure 3.12.** High density polyethylene tanks for the corrosion test. A pump was used to maintain the concentration of the NaCl solution.



**Figure 3.13.** Specimens corresponding to each sand type were kept separately to avoid interaction during the test.

### 3.3.6 Expansion of Mortar Bars due to ISA and DEF

Assessments of the potential for the sands to initiate deleterious expansion were assessed by tests performed on mortar bars. For ISA, tests were performed according to ASTM C1038 limewater exposure conditions (in separate containers for each sample group, to avoid contamination), with all samples prepared at a common water-to-cement ratio and expansions measured periodically. Other researchers have also employed ASTM C1038 or a similar test for assessments of contaminated sands [Atahan and Dikme, 2010; Kheder and Assi, 2010; Atahan and Dikme, 2011]. In addition, to assess the potential for DEF, replicate mortar samples were initially cured at high temperature according to the Kelham procedure and were subsequently soaked in separate limewater baths (ASTM C1038), with expansion measurements made periodically. Because the

ASTM C1038 test was designed to assess sulfate contents in cement, rather than sand, the test be performed for 6 months, to better evaluate the likely slower reaction kinetics in sand.

Ten bars and twelve cubes were prepared, using the mixture design in Table 3.4, using the procedure given by ASTM C305, for Cements A-E. For each batch of mortar, half were cured in moist containers at room temperature after casting to evaluate the occurrence of ISA (Figures 3.14 to 3.16), and half of the elements were exposed to the Kelham curing cycle, explained in Chapter 2, to assess the potential for DEF. To avoid evaporation of water during the high temperature regime, the containers were sealed. Also, a metallic grid was used to separate the water and the mortar samples. After these trays were removed from the oven, the presence of water inside the containers was confirmed to avoid the exposure of the samples to undesired effects, such as drying or plastic shrinkage.

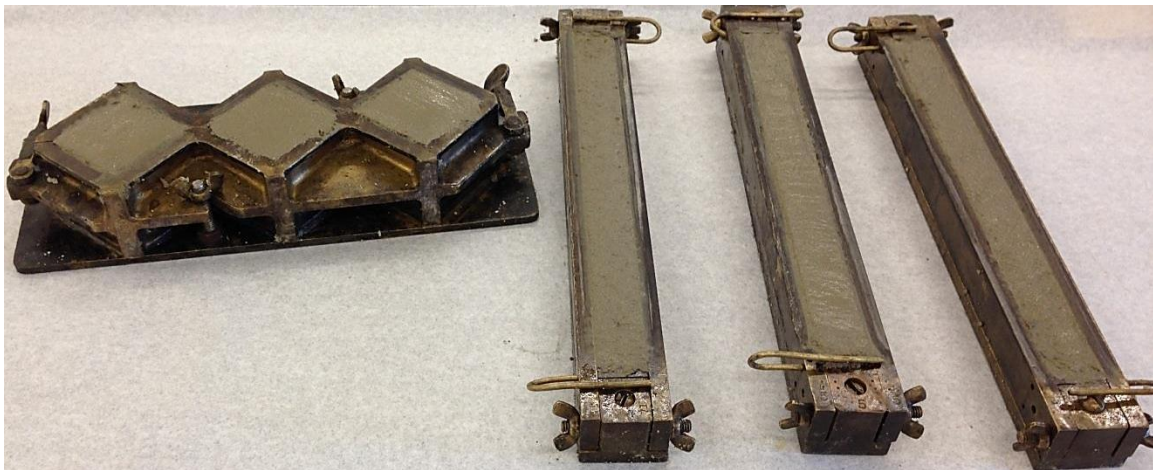


**Figure 3.14.** Mortar bars for length change testing and mortar cubes for compressive strength evaluation over time.

After 24 hours, the initial length of the mortar bars was measured using an apparatus conforming to ASTM C490, including a digital dial gauge with a precision of 0.002 mm ( $7.87402 \times 10^{-5}$  in). Then, they were stored in limewater in separate containers to avoid leaching and cross interaction between different specimens. Periodic measurements of the length of the bars were recorded on time using the same apparatus, under lab temperature ( $23 \pm 3$  °C) and humidity ( $50 \pm 15\%$ ). Before every measurement, the specimens were rotated gently until the reading from the dial stabilized. Every measurement was performed in the same position and orientation of the bar, to minimize the noise in the determination of the length change of the samples.

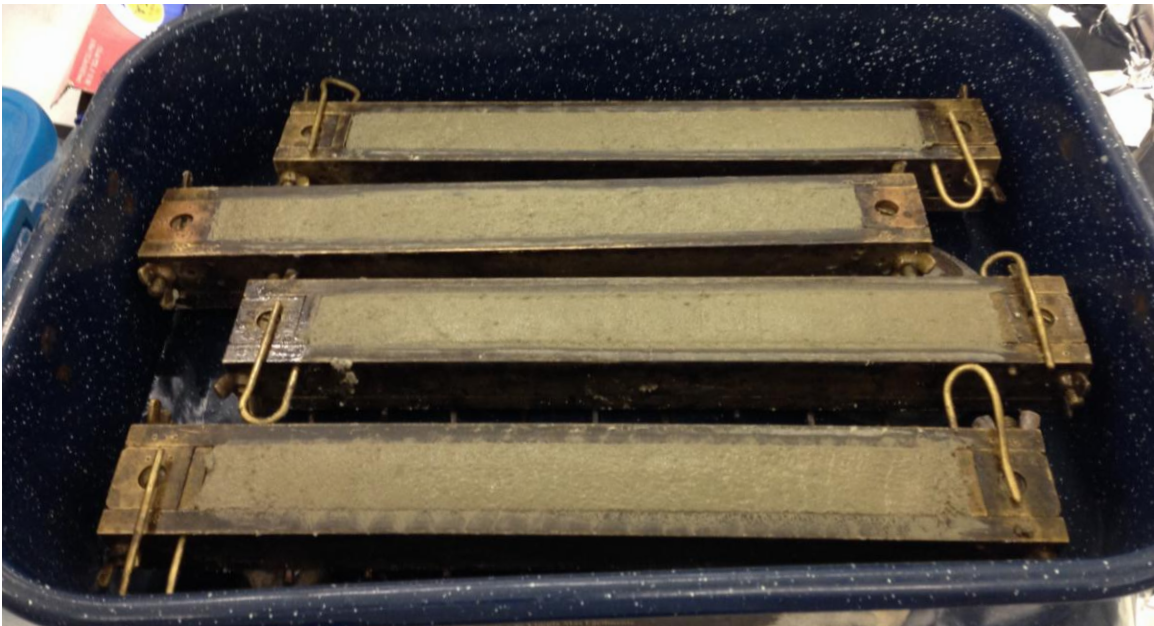


**Figure 3.15.** Metallic tray used to provide a moist condition during Kelham curing cycle.



**Figure 3.16.** Mortar samples were kept in a moist environment for the first 24 hours after casting. Aluminum foil was used to avoid water evaporation during Kelham curing cycle.



**Figure 3.17.** Compression frame used for strength assessment of mortar cubes.

## 4. EFFECT ON EARLY-AGE PROPERTIES

Sulfate, commonly as calcium sulfate dihydrate or gypsum, is commonly added to portland cement clinker to control the occurrence of flash set, a result of the very fast hydration of  $C_3A$ . The behavior at early age not only depends on the amount of gypsum added, but also on the  $C_3A$  content and reactivity. The amount and type of calcium aluminate hydrates formed is highly dependent on the sulfate-to- $C_3A$  ratio [Mindess et al., 2003]. Therefore, the potential for additional sources of sulfate (or sulfide), as well as the effect of aggregate acidity, to affect early hydration and setting should be evaluated.

In order to evaluate the effect of the additional sulfate or sulfide provided by Site H and Site D sands, setting times are evaluated by the Vicat needle test and the heat evolution during the first days is measured using isothermal calorimetry.

### 4.1 Setting Time by Vicat Needle Test

Two specimens were tested per mixture of mortar, prepared from Cement A (Type I/II cement) and each of the sand sources. Negligible differences were observed between duplicate specimens in the determination of the initial and final setting using a single cement source. Initial setting represents the beginning of the solidification of the cement paste and the point when a limited workability affects considerably concrete operations, such as placement and finishing. Final setting represents the point when the solidification process is finished, and the paste starts to develop stiffness [Mehta and Monteiro, 2006].

The source of sand used clearly affects the setting time. The setting times of mortar including Cement A and Site D and H sands show delays in initial and final setting compared to control mortar (see Figure 4.1). Site D sand exhibits a delay of the initial setting of 51 minutes and a delay of the final setting of 25 minutes, while Site H sand delays initial setting in 67 minutes and delays final setting in 85 minutes with respect to control samples.

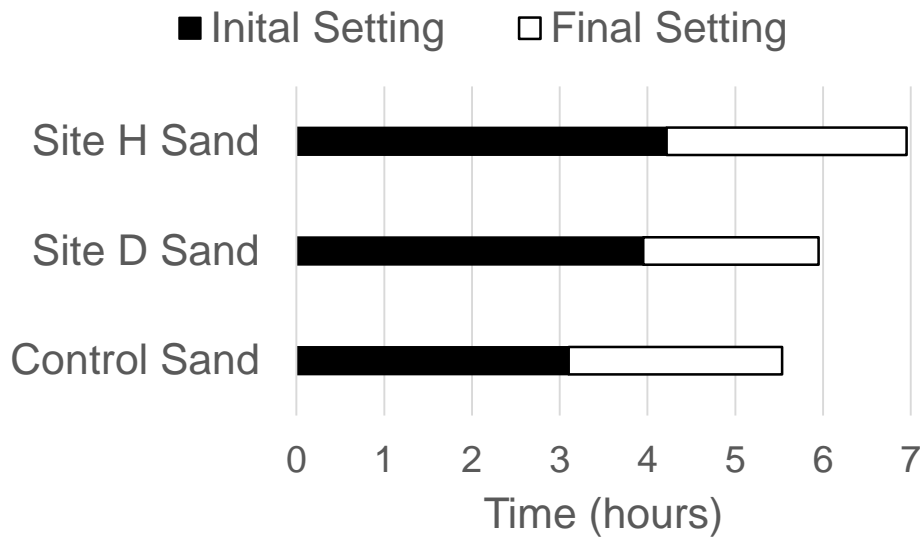


**Figure 4.1.** Initial and final setting times of mortars prepared using Cement A.

The delays observed in Site H and D sand samples suggest that the composition of the sands influence the cement setting behavior. One possibility is that the presence of sulfate or sulfide delays the hydration. Additional sulfates from the sands, then, could lead to additional retardation in hydration reactions. Variation in setting time could be a concern for construction operations and early strength development.

## 4.2 Isothermal Calorimetry

Isothermal calorimetry at 25 °C was performed on mortar mixtures using Cements A, B, and C, with mortars prepared at w/c of 0.5 (see Table 3.3). Tests were conducted on three replicates per mixture. Calorimetric curves are a measure of the heat evolved by exothermic reactions, provided at early ages mostly by the initial cement dissolution and the early hydration of C<sub>3</sub>S and C<sub>3</sub>A. Figures 4.2 to 4.4 show heat evolution curves for the first 40 hours of hydration for each of three cements as mortars with each of the three sand sources.

It can be observed that hydration of all three cements is delayed most in the presence of Site H sand, which has the higher sulfate content than Site D sand. Site D sand shows an intermediate behavior between control and Site H sand, but is still delayed with respect to the control.

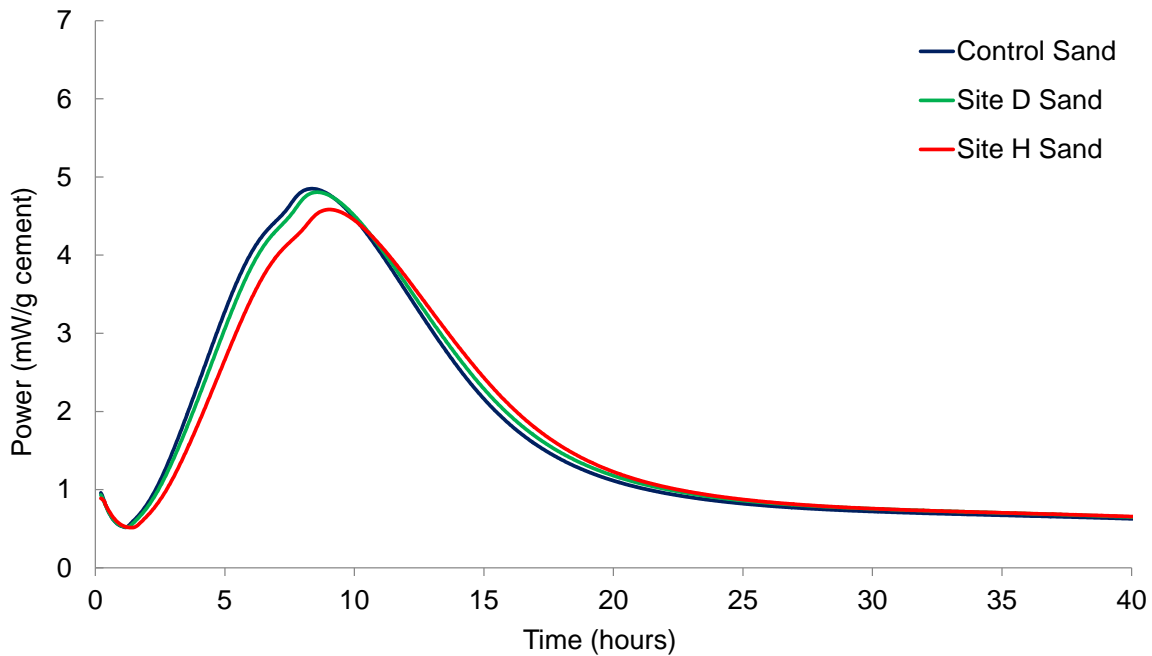


**Figure 4.2.** Calorimetry results for mortar mixtures prepared with Cement A.

For Cement A (Figure 4.2), use of Site H sand results in a delay in the maximum peak of hydration, which occurs at 9.1 hours instead of 8.4 hours (as observed in the control). This is consistent with the results of setting time for the same cement (Figure 4.1). With the Site D sand, the maximum peak occurs at 8.6 hours, which is a more moderate retardation but is also appreciable in this test.

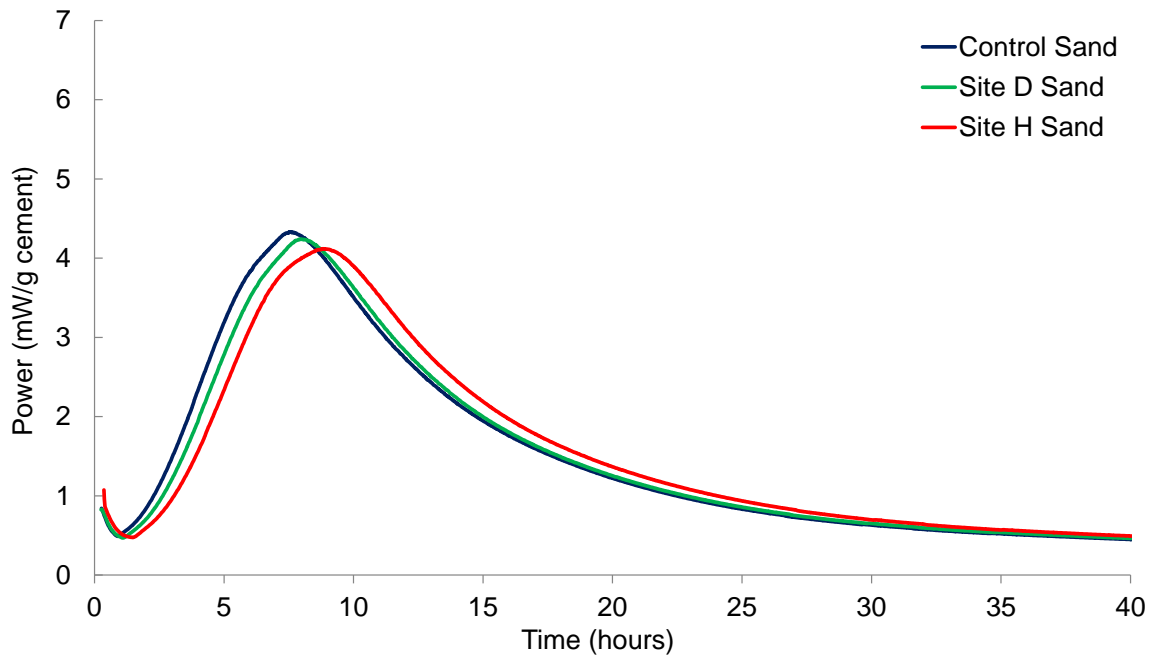


**Figure 4.3.** Calorimetry results for mortar mixtures prepared with Cement B.

For Cement B (Figure 4.3), a Type V cement with lower  $C_3A$  (2.97% compared to 6.50%) and  $C_3S$  (54.50% compared to 62.08%) contents than Cement A, the delay is more pronounced when acidic sands are used. Site H sand delays the peak of hydration from 7.5 hours to 8.8 hours, while Site D sand exhibits the maximum peak at 8 hours. Cement B has a higher  $SO_3/C_3A$  ratio than Cement A (0.79 and 0.39, respectively),

suggesting that the addition of sulfate from the sand source will produce a stronger effect on the heat of hydration at early-age, particularly given the lower amount of  $C_3A$ .

Cement C (Figure 4.4) has a higher sulfate content than Cement A, but also a higher amount of  $C_3A$ . For Cement C, the  $SO_3/C_3A$  is 0.47, compared to 0.39 for Cement A. The maximum peaks were at 5.8 hours for control sand, 6.1 hours for Site D sand, and 6.4 hours for Site H sand. These results suggest that when the sulfate content of the cement is higher, relative to the calcium aluminate content, that any additional sources of sulfate or sulfide for the sand are less likely to retard early hydration as measured by calorimetry.

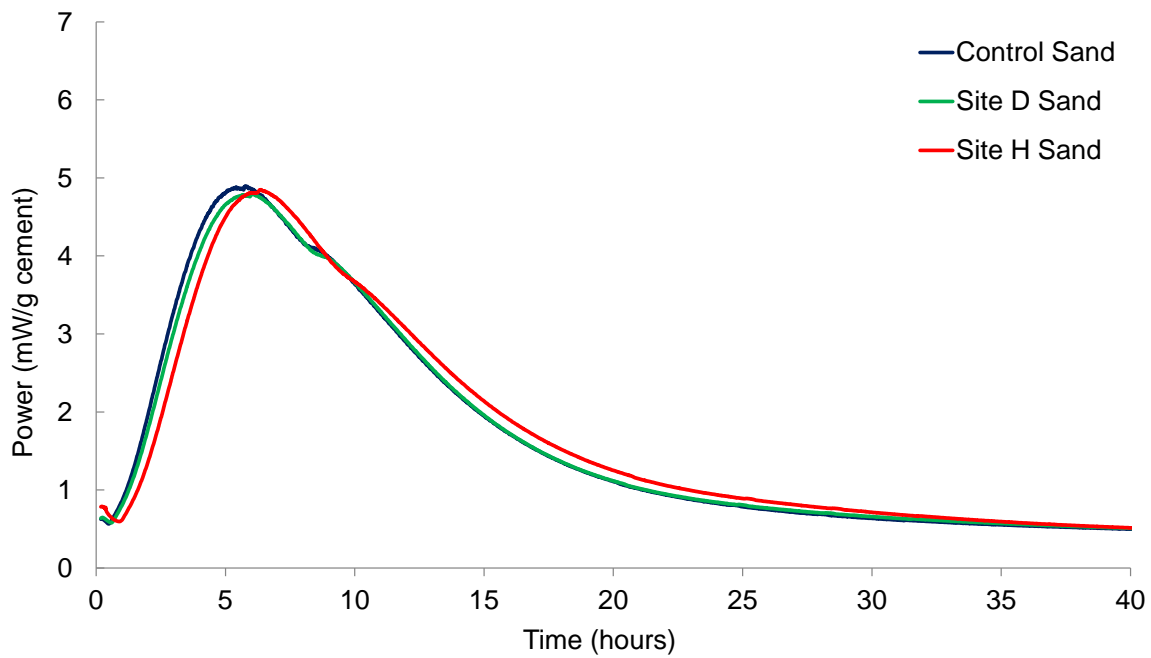


**Figure 4.4.** Calorimetry results for mortar mixtures prepared with Cement C.

The curves for the total heat evolved (Figure 4.5) show that the heat of hydration after 72 hours has a similar value for every type of sand. (Plots for each cement are

shown individually in Appendix A.) These data suggest that beyond 3 days, any delays in hydration due to minor constituents in the sand are likely to be less apparent. The total heat is clearly higher for Cement A and C, likely due to a higher amount of  $C_3A$  and  $C_3S$  in these cements relative to Cement B. Also, for Cement B and C, the total heat of Site H samples after 72 hours is slightly higher compared to Site D sand and control samples.

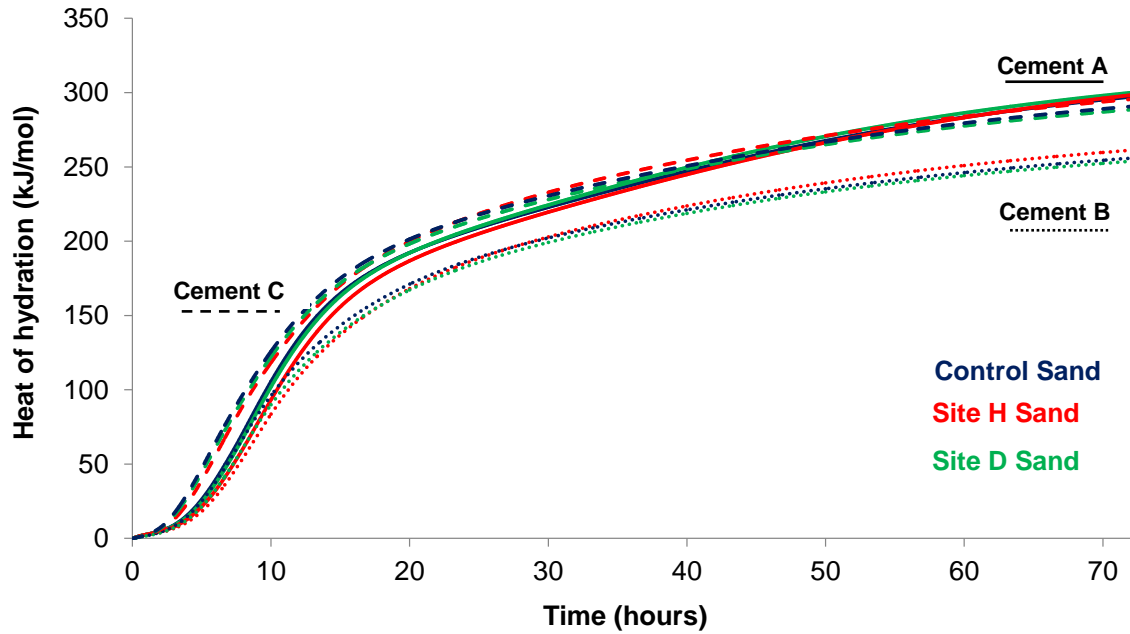


**Figure 4.5.** Cumulative heat of hydration curves for the first 72 hours.

## 5. EFFECT ON MECHANICAL PROPERTIES OF CONCRETE

In Chapter 4, it was demonstrated that minor constituents in the sand can delay early hydration and lead to increased time to set, with the relative magnitude of these effects related to the cement composition. This chapter examines whether such interactions are manifested in mechanical properties. Specifically, compressive strength and dynamic modulus are measured for concretes containing each of the three sand sources.

### 5.1 Compressive Strength Results

Figure 5.1 shows the average compressive strength measured at ages 1, 3, 7, 28, 56, and 91 days for concrete mixtures using each type of sand. All concretes were prepared at w/c 0.43 using Cement A (Type I/II cement). These mixes conformed to GDOT AA1 specifications (Table 3.5). Individual results of the test for each cylinder can be observed in Appendix B, along with the average and standard deviation for each sand and age.

Table 5.1 shows the results of the statistical analysis on the statistical similarity of the results for the acidic sand ( $\mu_h$  and  $\mu_d$ ) with respect to control sand ( $\mu_c$ ), where  $\mu_i$  is the mean of the normal distribution of compressive strength of sand  $i$ , at a particular age. For each hypothesis testing, the table shows the decision of the test for  $\alpha = 5\%$  and the p-value. The p-value is the conditional probability of rejecting  $H_0$  given that  $H_0$  is true. Thus, a low p-value indicates that the occurrence of  $H_0$  is very unlikely, and this assumption is consequently rejected.

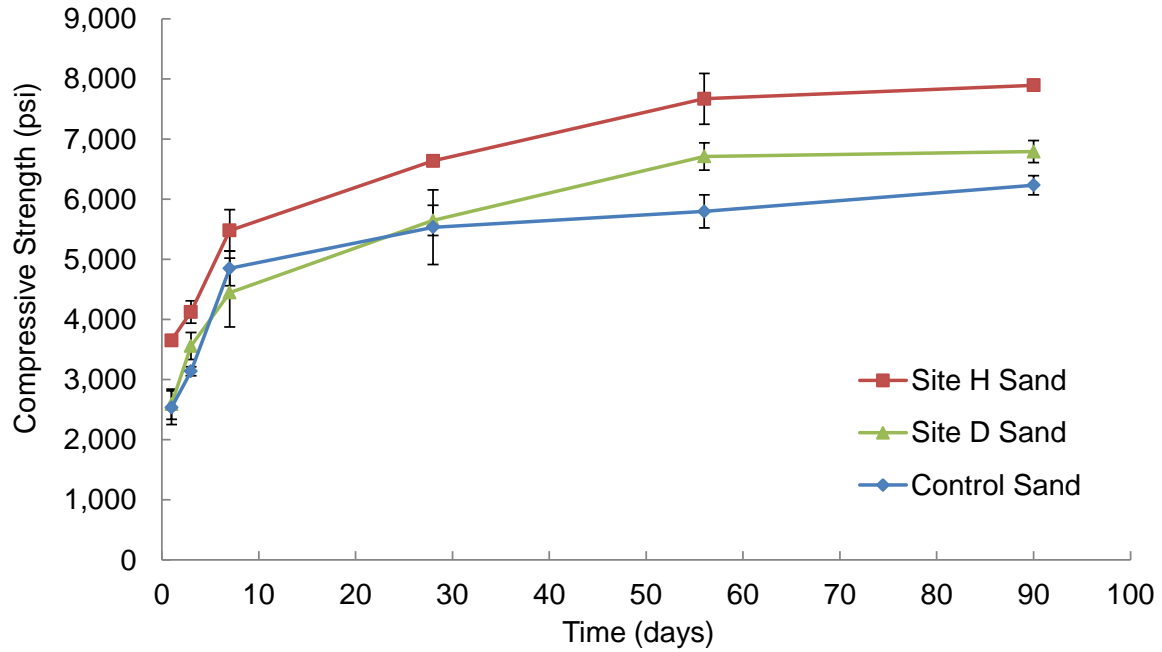


**Figure 5.1.** Average compressive strength of concrete at 1, 3, 7, 28, 56, and 90 days after casting. Each point corresponds to the average of three cylinders and the error bars show the standard deviation.

**Table 5.1.** Statistical analysis of compressive strength results. Similarity of the results observed using acidic sands compared to control is tested.

Age of Testing	Test $H_0: \mu_c = \mu_h$ ( $\alpha = 5\%$ )	p-value	Test $H_0: \mu_c = \mu_d$ ( $\alpha = 5\%$ )	p-value
1 day	Reject $H_0$	0.673%	Fail to Reject $H_0$	96.365%
3 days	Reject $H_0$	0.072%	Fail to Reject $H_0$	9.133%
7 days	Fail to Reject $H_0$	6.278%	Fail to Reject $H_0$	59.856%
28 days	Reject $H_0$	3.089%	Fail to Reject $H_0$	95.790%
56 days	Reject $H_0$	0.214%	Reject $H_0$	2.775%
90 days	Reject $H_0$	0.005%	Fail to Reject $H_0$	40.129%

Samples using Site H sand show a higher strength compared to control samples, except at 7 days. Concretes using Site D sand show statistically different behavior. At early ages (i.e., up to 28 days), concretes containing control and Site D sand exhibit statistically similar compressive strength. At later ages, the results show a higher value for Site D sand at 56 days, but similar at 90 days.

Repeating the statistical analysis performed between the concretes produced with Site D and H sands, Table 5.2 indicates that the compressive strength of Site H samples is higher compared to Site D samples, at every age of testing. Because Site D and H sands were obtained from the same source, the variability in the concrete compressive strength is a concern. The inconsistency of the sand source and its influence on strength should be quantified, for a range of concrete mixture designs and for a range of cement compositions.

**Table 5.2.** Variability between Site H and Site D sand samples.

Age of Testing	Test $H_0: \mu_d = \mu_h$ ( $\alpha = 5\%$ )	p-value
1 day	Reject $H_0$	0.584%
3 days	Reject $H_0$	2.177%
7 days	Reject $H_0$	4.799%
28 days	Reject $H_0$	0.177%
56 days	Reject $H_0$	2.020%
90 days	Reject $H_0$	0.262%

Additionally, GDOT Specification 500 mandates that AA1 concrete have a 28-day compressive strength higher than  $f'_c + 2 \cdot s$ , where  $f'_c$  and  $s$  are obtained from tables and correspond, in the case of AA1 mixtures, to 4,500 psi and 540 psi, respectively. Therefore, the minimum required 28-day strength is 5,580 psi. The averages of samples prepared using Site H and Site D sands are higher than this value, while the average for control sand samples at the same age is slightly lower (see Appendix B). At 28 days, control sand samples show a standard deviation of 621 psi, which is higher than specified by GDOT.

### **5.1 Dynamic Elastic Modulus Results**

The dynamic elastic modulus of concrete was tested at 28 and 90 days of age. Results are shown in Table 5.3. Similar to the compressive strength results at these ages, the Site H sand concretes show highest values of dynamic modulus at both ages examined. Based upon statistical analysis, results for Site D and control sand samples are similar, while results of dynamic elastic modulus of concrete produced from Site H do not show statistical evidence to conclude similarity with the ones observed for control concrete (Table 5.4). Again, the variability in behavior for concrete with Site D and Site H sand – where the modulus of the Site D concrete is statistically similar to the control, but the Site H concrete is not – may be a concern. The inconsistency of the sand source and its influence on modulus should be quantified, for a range of concrete mixture designs and for a range of cement compositions.

**Table 5.3.** Dynamic elastic modulus at 28 and 90 days.

	<b>Dynamic E @ 28 days, ksi</b>	<b>Std Dev, ksi</b>	<b>Dynamic E @ 90 days, ksi</b>	<b>Std Dev, ksi</b>
Control Sand	<b>5,200</b>	80	<b>5,331</b>	224
Site H Sand	<b>5,505</b>	90	<b>5,764</b>	160
Site D Sand	<b>5,386</b>	37	<b>5,671</b>	108

**Table 5.4.** Statistical analysis of dynamic elastic modulus results.

Age of Testing	<b>Test H<sub>0</sub>: <math>\mu_c = \mu_h</math> (<math>\alpha = 5\%</math>)</b>	<b>p-value</b>	<b>Test H<sub>0</sub>: <math>\mu_c = \mu_d</math> (<math>\alpha = 5\%</math>)</b>	<b>p-value</b>
28 days	Reject H <sub>0</sub>	0.879%	Fail to Reject H <sub>0</sub>	5.346%
90 days	Reject H <sub>0</sub>	4.519%	Fail to Reject H <sub>0</sub>	17.423%

The dynamic elastic modulus is an estimation of the static elastic modulus by non-destructive methods (NDT). The static elastic modulus is consistently lower than the dynamic elastic modulus, but a linear correlation has been observed in experimental values obtained for both mechanical properties [Popovics et al., 2008]. However, the selection of the equation to relate both values will depend on parameters such as the test used to determine the dynamic modulus, the geometry of the specimens, or the vibration mode [Popovics et al., 2008]. This difference between the static and dynamic elastic moduli is a consequence of the composite nature of concrete, being the results obtained for each property consistent with different composite phase models. According to Popovics et al. [2008], the best agreement between the dynamic elastic modulus obtained

by ASTM C215, using longitudinal vibration of cylinders, and the static elastic modulus obtained by ASTM C469 is the British Standard equation (BS8110, Part 2):

$$E_s = 1.25 \cdot E_d - 19 \quad (9)$$

where  $E_s$  and  $E_d$  correspond to the static and dynamic moduli, respectively, in GPa.

The value for the static modulus of elasticity can also be calculated from ACI 318-11: Building Code Requirements for Structural Concrete and Commentary, using the compressive strength of concrete. A comparison between these calculations is shown in Table 5.5. GDOT Section 500 does not address requirements for elastic or dynamic modulus of concrete.

**Table 5.5.** Estimations of the static modulus of elasticity from ACI 318 and BS 8110 equations.

	Age	Control Sand	Site H Sand	Site D Sand
<b>Static E</b> ACI 318 (ksi)	28 d	4,240	4,644	4,283
	90 d	4,499	5,065	4,627
<b>Static E</b> BS 8110 (ksi)	28 d	3,744	4,126	3,977
	90 d	3,908	4,450	4,333

## **6. EFFECT ON DURABILITY**

One of the main aspects of this project was to assess the effect of sulfate/sulfide-bearing sands on the long-term performance of mortar and concrete. Particularly, the potential influence of low pH and minor mineral components associated with the Site D and H sands to influence durability of concrete related to corrosion resistance and potential for deleterious sulfate attack, by ISA or DEF, were examined. In addition, results from standard testing of concrete mixtures by rapid chloride permeability are presented in this chapter.

### **6.1 Rapid Chloride Penetration Test Results (RCPT)**

Rapid Chloride Penetration Testing (RCPT), as performed by ASTM C1202, provides an indication of the quality of the concrete, as measured by the charge passed (measured in Coulombs, C) across a saturated concrete specimen. Here, two concrete samples prepared with Cement A and w/c of 0.43 (see mixture design in Table 3.5), were tested for each source of sand. For all three concrete mixtures, the RCPT results measured at 56 days of age after fogroom curing correspond to moderate permeability.

**Table 6.1.** Total charge passed during RCPT performed at 56 days of age.

Sample	Charge Passed, Coulombs		Chloride Ion Penetrability
	Average	Std Dev	
Control Sand	<b>3,975</b>	345	Moderate
Site D – Sand	<b>3,064</b>	577	Moderate
Site H – Sand	<b>3,354</b>	634	Moderate

Site D and Site H sands show a lower charge passed, compared to the control concrete (Table 6.1). Filling of pores or microcracks by secondary products, such as ettringite, could contribute to a lower charge passed during this test. The variability among the Site D concrete and Site H concrete, as measured by standard deviation in these tests, is also greater than the control. Again, further testing to consider different concrete mixture proportions and cementitious materials compositions, as well as different ages of testing, should be performed to better understand the influence of sand source on RCPT values and the implications for long-term durability.

## **6.2 Accelerated Corrosion Test**

Corrosion activity of each concrete-embedded steel bar was measured in terms of the current flowing between the counter electrode and the embedded bar, as described in FM 5-522. The results of the corrosion test can be observed in Figure 6.1, which shows the average current measured during the testing.

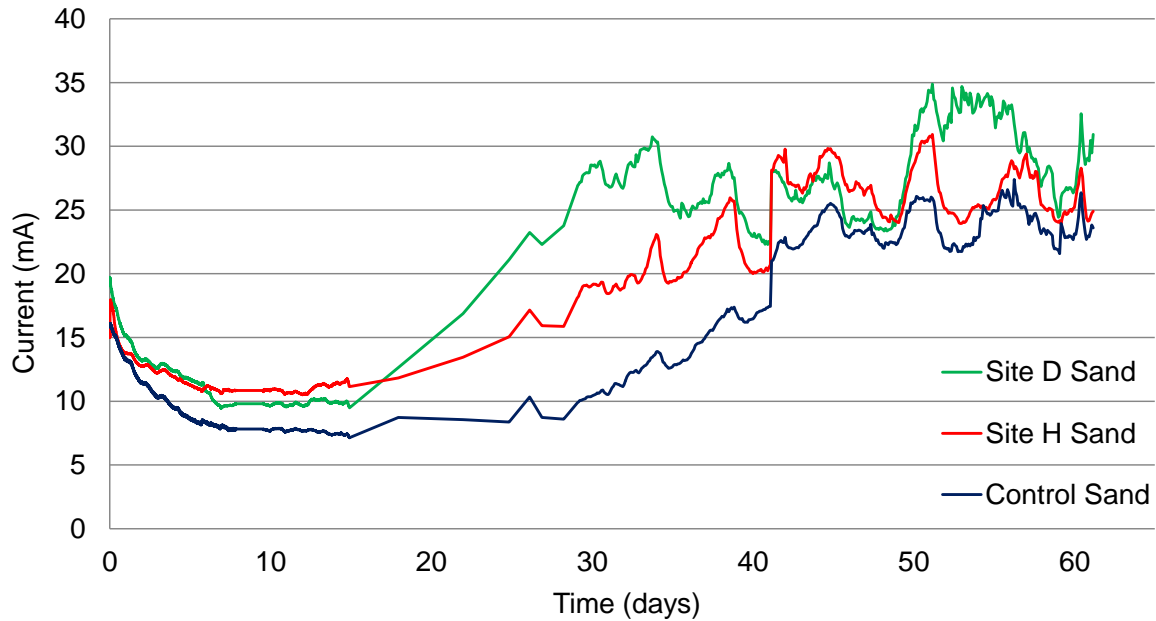


**Figure 6.1.** Current over time for concrete samples exposed to a NaCl solution. Every line represents the average of three specimens.

The voltage applied during the test was measured and controlled. An average value of 5.998 V was recorded during the 60 days of the test at the start and at the end of the circuit. The maximum and minimum voltages were 6.059 and 5.918 V, respectively. An initial reduction in the current is due to the stabilization of the passive layer of the embedded steel in all tested concrete samples, followed by a plateau. This plateau corresponds to the average daily current,  $I_{avg}$ .

After ~15 days, an increment of the current for Site D and Site H samples indicates an increase in the corrosion activity for these embedded steel-bar surfaces due to the destabilization of the passive layer, exposing active steel that corrodes at a faster rate. After ~28 days, the control samples also show this increment (i.e., an abrupt change of slope). The measured current is a function of the corrosion rate of the embedded steel.

These tests were repeated two times under the same conditions, and the results coincided in terms of the time to corrosion initiation, magnitude of current, and evolution of current over time (see Appendix C: Figure C.1). Also, Table 6.2 shows the calculated average daily resistance of every sand type. Site H and D specimens show higher current during the entire test period.

**Table 6.2.** Average resistance and time to failure of concrete samples for the corrosion test.

	<b>Average daily resistance (<math>R_{avg}</math>), Ohm</b>	<b>Time-to-failure, days</b>
Control Sand	776.6	28.23
Site D Sand	607.3	14.84
Site H Sand	550.4	14.86

These results indicate that the use of Site H and Site D sands accelerates the corrosion initiation of the reinforcement. This statement was qualitatively corroborated with the visual evaluation of the deterioration of the samples over time. Samples including Site D and Site H sands exhibited more extensive formation of corrosion products, surface discoloration, and cracking compared to control samples. At day 30 from the start of the current monitoring, the extent of cracking and corrosion products was considerable for the samples with Site H and D sands. Figures 6.2 to 6.4 show the evolution of damage for the samples during the test.

This result, along with the pH evolution with time (Figure 3.3), suggests that the pyrite content – or at least the influence of the pyrite content – in Site D sand could be

similar to the reported for Site H sand. The variability of the current evolution among different specimens of the same type of sand is shown in Appendix C: Figures C.2 to C.4.

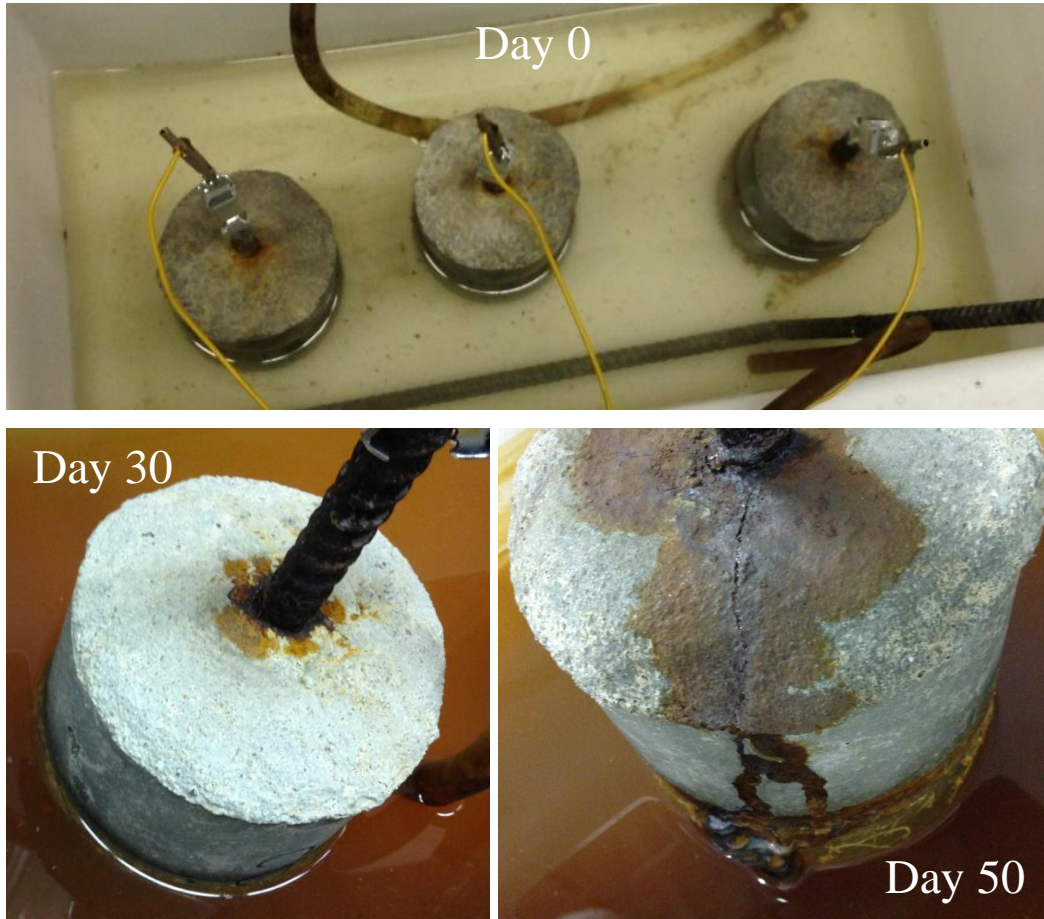
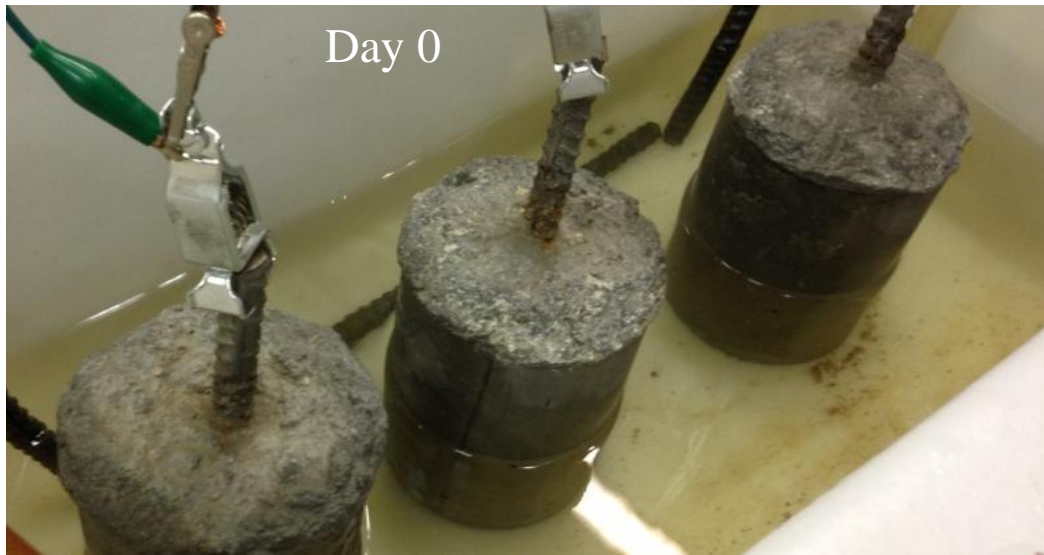


**Figure 6.2.** Specimens for Control Sand at 0, 30, and 50 days from the start of the test.



Day 0



Day 30



Day 50



Day 50

**Figure 6.3.** Specimens for Site D Sand at 0, 30, and 50 days from the start of the test.



**Figure 6.4.** Specimens for Site H Sand at 0, 30, and 50 days from the start of the test.

#### **6.4 Potential for Internal Sulfate Attack (ISA)**

Assessment of the potential expansion due to ISA was performed in mortar bars, using five different cements (A-E), prepared with w/c of 0.5 and sand/cement of 2.75. Mortars were prepared using Site H sand and control sand. (Site H was selected for this comparison due to its higher sulfate content.) After casting, the samples were cured in sealed containers at RH of ~100% and at room temperature for 24 hours. Then, after demolding, mortars were stored in limewater, in sealed containers at room temperature.

Cements A, B, and C were used in samples cast near the start of the project, while Cements D and E were included later in order to broaden the range of cement compositions in the study. Thus, the results for Cements D and E consider a 200-day testing period. The testing period was longer for Cement A, extending to 400 days. Results for Cements B and C extend to more than 390 days for Site H sand samples and to more than 275 days for control sand samples.

Figures 6.5 to 6.9 show the measurements of length change over the test period. In order to compare the magnitude of the expansions, the graphs have the same scale, with a maximum value of 0.1%.

After 24 hours of soaking, both sets of samples exhibited a minor expansion of ~0.006%, due to water absorption after limewater storage. After that, an almost negligible expansion of has been observed in all of the mortars examined. For the two sand sources and five cements examined, mortars prepared with Cement A and Site H sand exhibit the highest expansion, 0.021% at 434 days. This value is well below limits typically placed on mortars for deleterious expansion.

Additionally, Table 6.3 shows the compressive strength of mortar cubes at 28 and 100 days. Similar to the results of compressive strength of concrete (Section 5.1), there is an increase in strength over time.

The absence of damaging expansion and an increase in mortar strength over time indicate that ISA does not deleteriously affect mortar mixtures prepared with acidic sands within the time period examined or for the range of cement compositions examined.

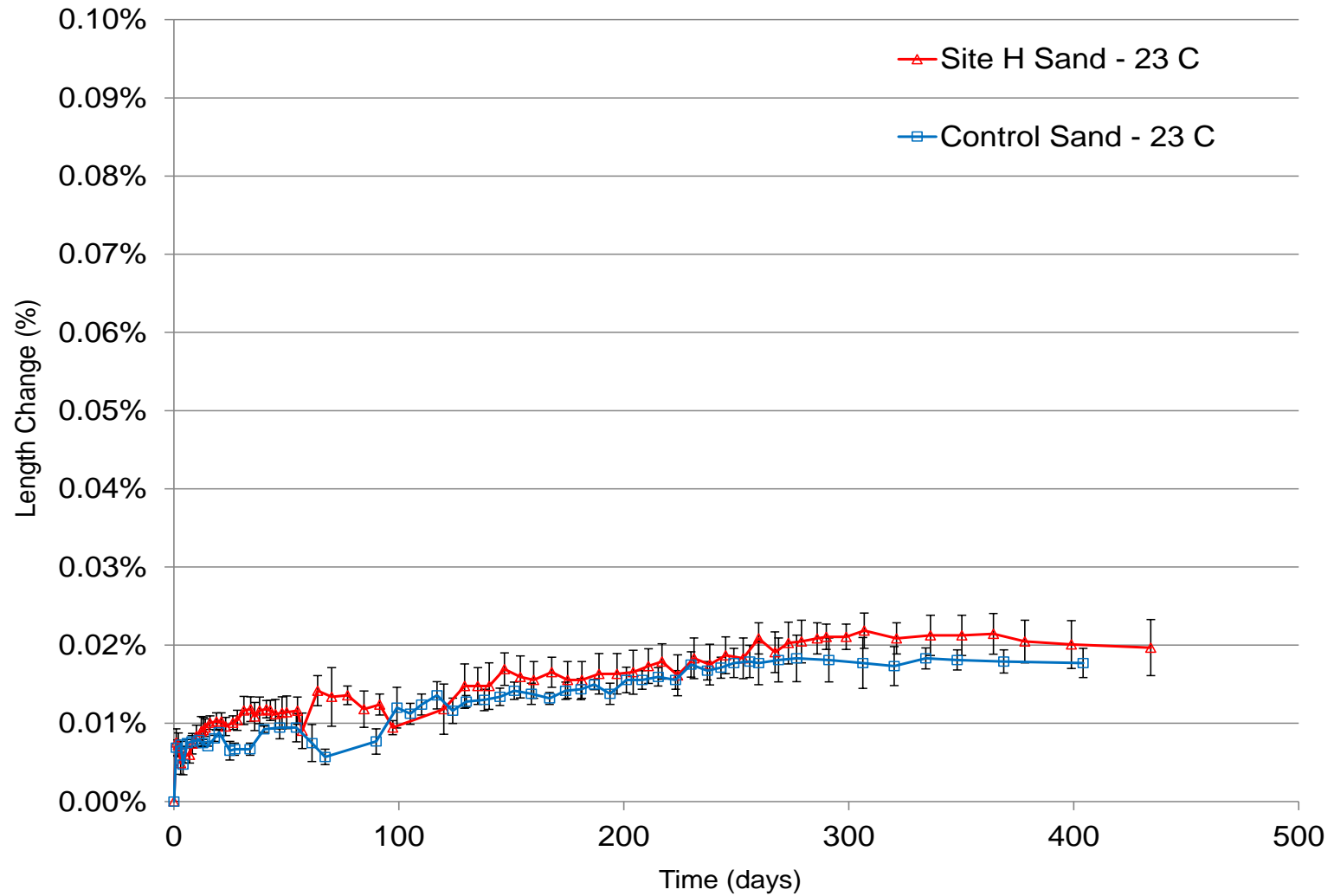


**Figure 6.5.** Expansion of mortar bars due to ISA (Cement A). Error bars represent standard deviation.

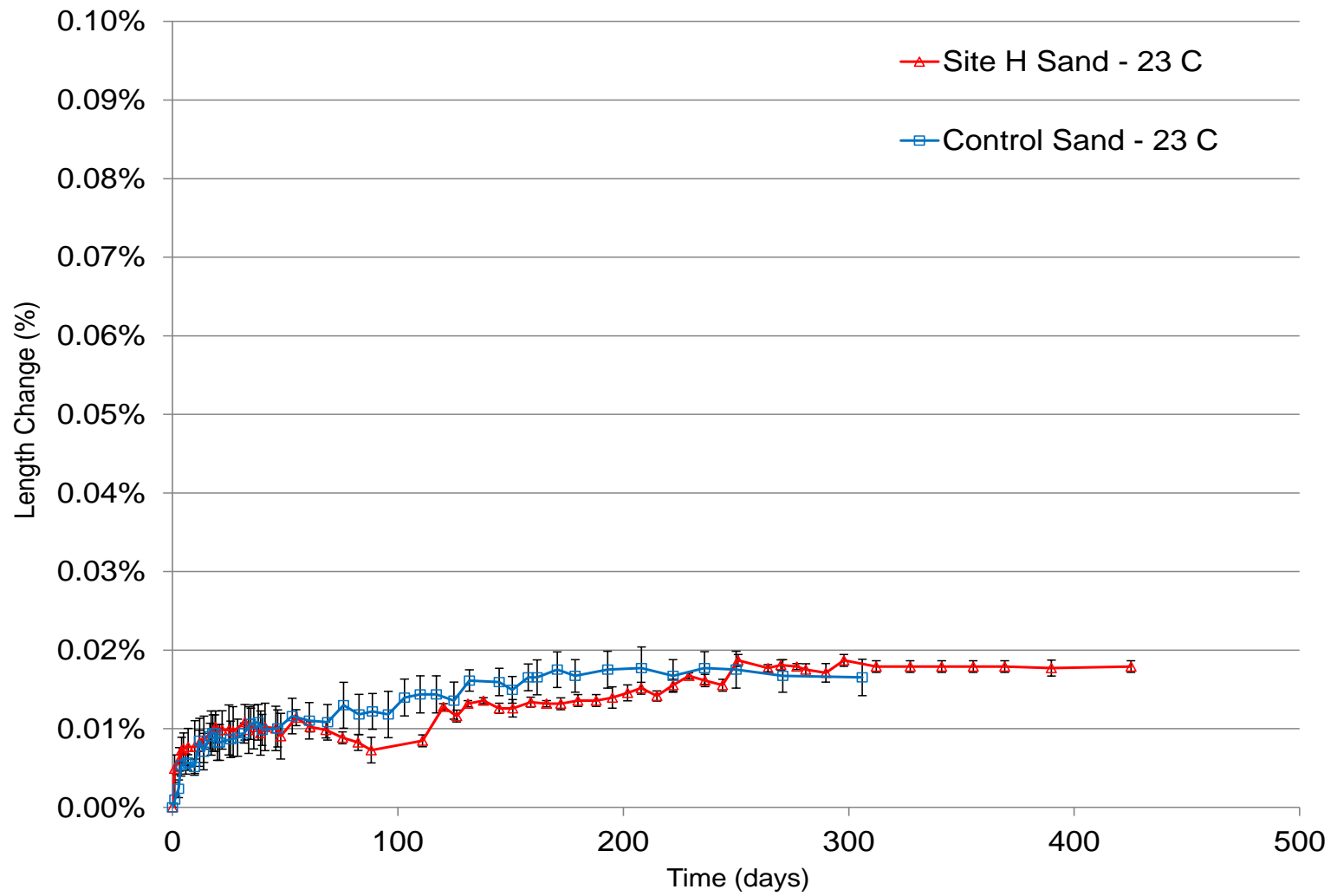


**Figure 6.6.** Expansion of mortar bars due to ISA (Cement B). Error bars represent standard deviation.

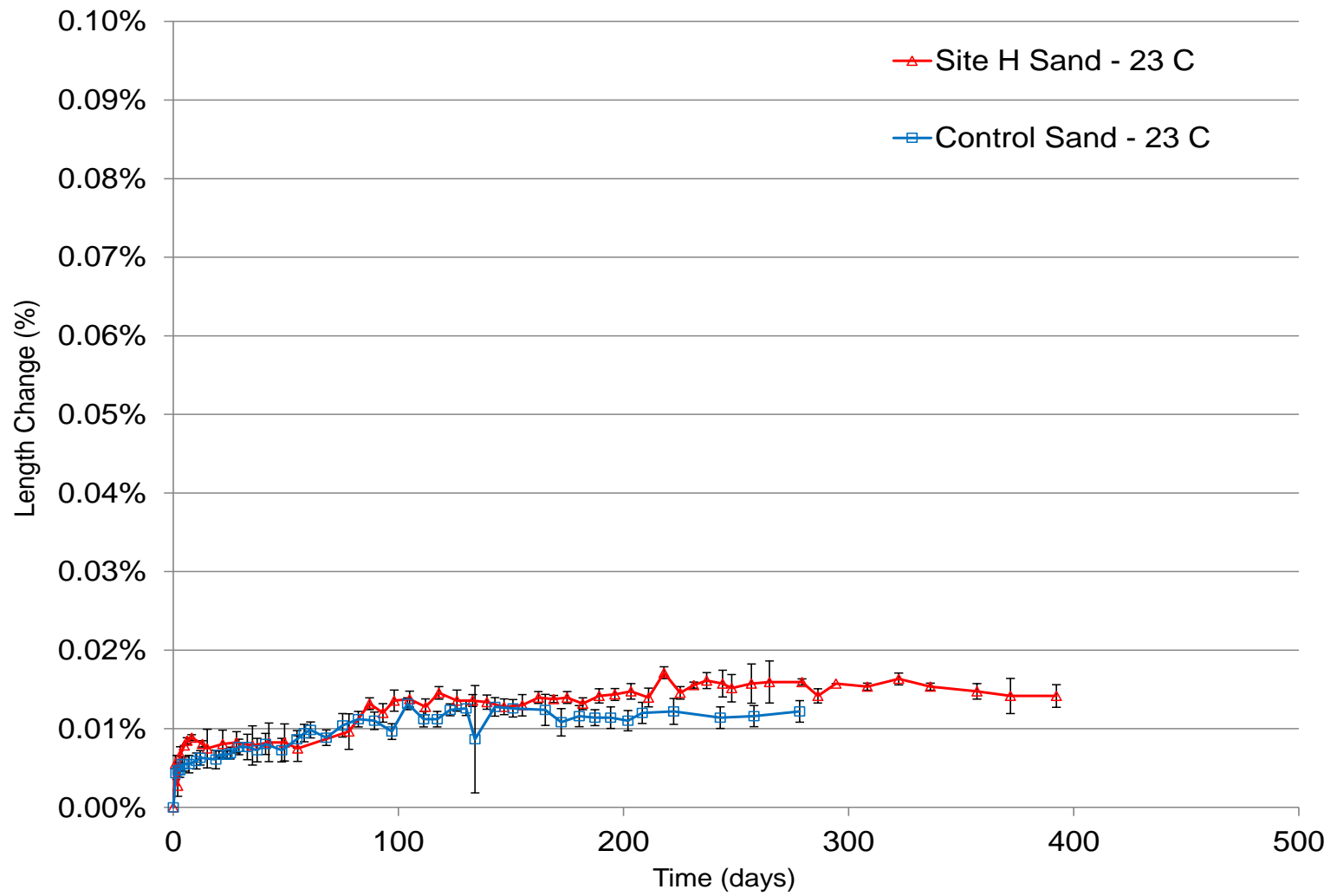


**Figure 6.7.** Expansion of mortar bars due to ISA (Cement C). Error bars represent standard deviation.

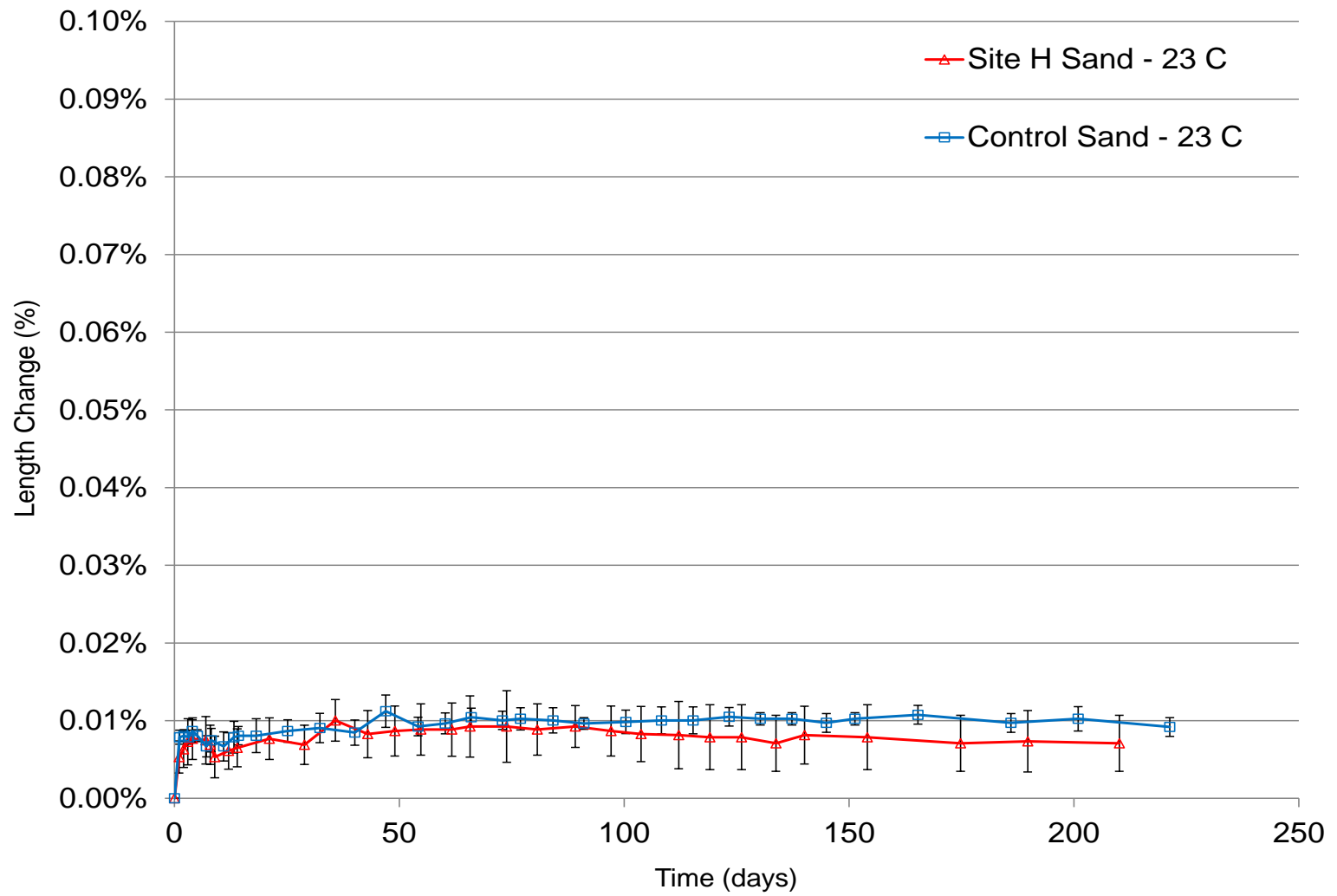


**Figure 6.8.** Expansion of mortar bars due to ISA (Cement D). Error bars represent standard deviation.

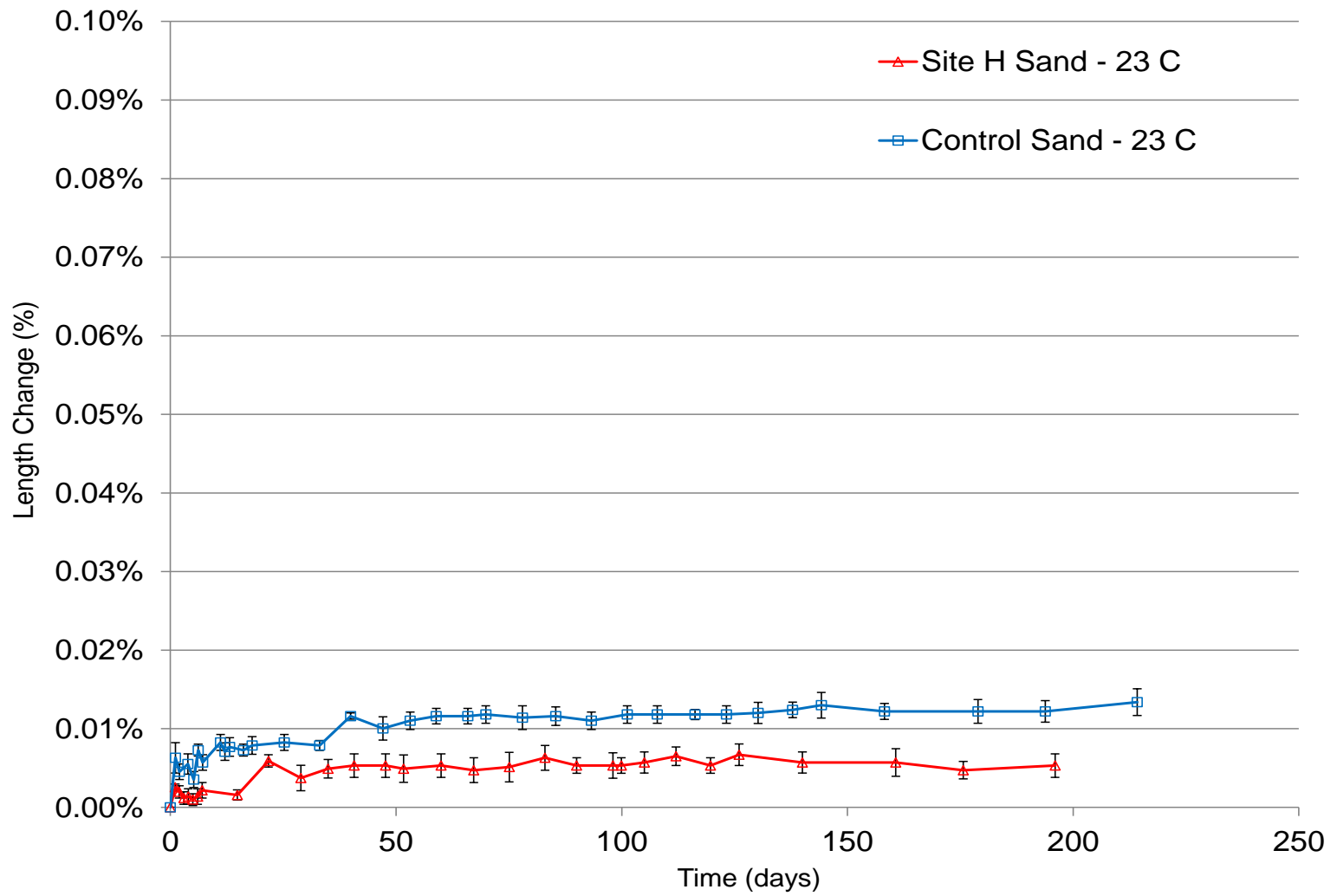


**Figure 6.9.** Expansion of mortar bars due to ISA (Cement E). Error bars represent standard deviation.

#### **6.4 Potential for Delayed Ettringite Formation (DEF)**

Potential for deleterious expansion by delayed ettringite formation was evaluated for heat-cured mortars, prepared from 5 different cements (A-E), and subsequently soaked in limewater at room temperature. As with the ISA testing, mortars were cast from Site H sand and control sand.

Partial expansion results are shown in Figures 6.10 to 6.14, corresponding to Cement A, B, C, D, and E. All the graphs have the same scale, except for Cement D, which exhibited the highest expansions. Graphs show results for Site H sand samples in red and control sand samples in blue. It should be noted that samples prepared using Cement D and E were cast more recently, and hence ~200 days of data are available currently compared to more than 300 days for Cements A, B, and C.

After twenty-four hours of limewater storage, control sand samples exposed to the Kelham curing method showed shrinkage of 0.004% to 0.010%. In contrast, expansion of 0.004 to 0.011% at 24 hours from demolding was observed for mortar bars prepared with Site H sand at this age.

All the samples exposed to high temperature curing cycle have exhibited expansion, except for samples using control sand and Cement B (Type V). For reference, the values for expansion have reached 7 to 24 times higher than the expansion limit of 0.1% used for alkali silica reaction in ASTM C1260 and for sulfate attack in ASTM C1012 experimental evaluation on the same type of bars. In fact, this expansion limit was reached as early as 33 days for Cement A mortars with Site H sand.

Generally, for Type I or I/II cement (Cements A, C, and E), Site H sand samples began to show expansion earlier than control sand samples, when subjected to heat

curing. Mortars with control sand in combination with these cements began to expand at later ages. Specimens with Cement A and Site H sand started expanding around day 5, while control samples started expanding at day 20. For Cement C, expansion started at day 15 and 48 for Site H and control sand, respectively. For Cement E (Type I cement, with higher  $C_3A$  content than Cement A), expansion started at day 16 and 25 for Site H and control sand, respectively. After expansion initiation, these samples exhibit a faster expansion rate (slope of the curve after expansion onset) when Site H sand is used. Cement A curves, which include a longer period of testing, show similar expansion measured later than day 120 and a considerable slower expansion rate for both types of sands.

For Cement B (Type V) mortar and control sand, the expansion was negligible and very similar to the one observed in samples cured at room temperature (see Section 6.4). The use of sulfate-resisting Cement B in combination with Site H sand produces expansion, but at a considerable slower rate compared with the rest of the cements. At 425 days, samples cast with Cement B and Site H sand expanded 0.113%. In comparison, for the same sand combined with ordinary Cement A, expansion measured nearly seven times more, or 0.773%, at 434 days.

In the case of Cement D (Type III), a very fast expansion and similar behavior between Site H sand and control sand samples are observed. This is likely due to the high availability of sulfate (from the sand) and alumina (from the cement). After the fast expansion period, Site H sand samples have expanded at a higher rate than control samples. Thus, a higher maximum expansion is expected for mortar including Site H sand and Cement D.

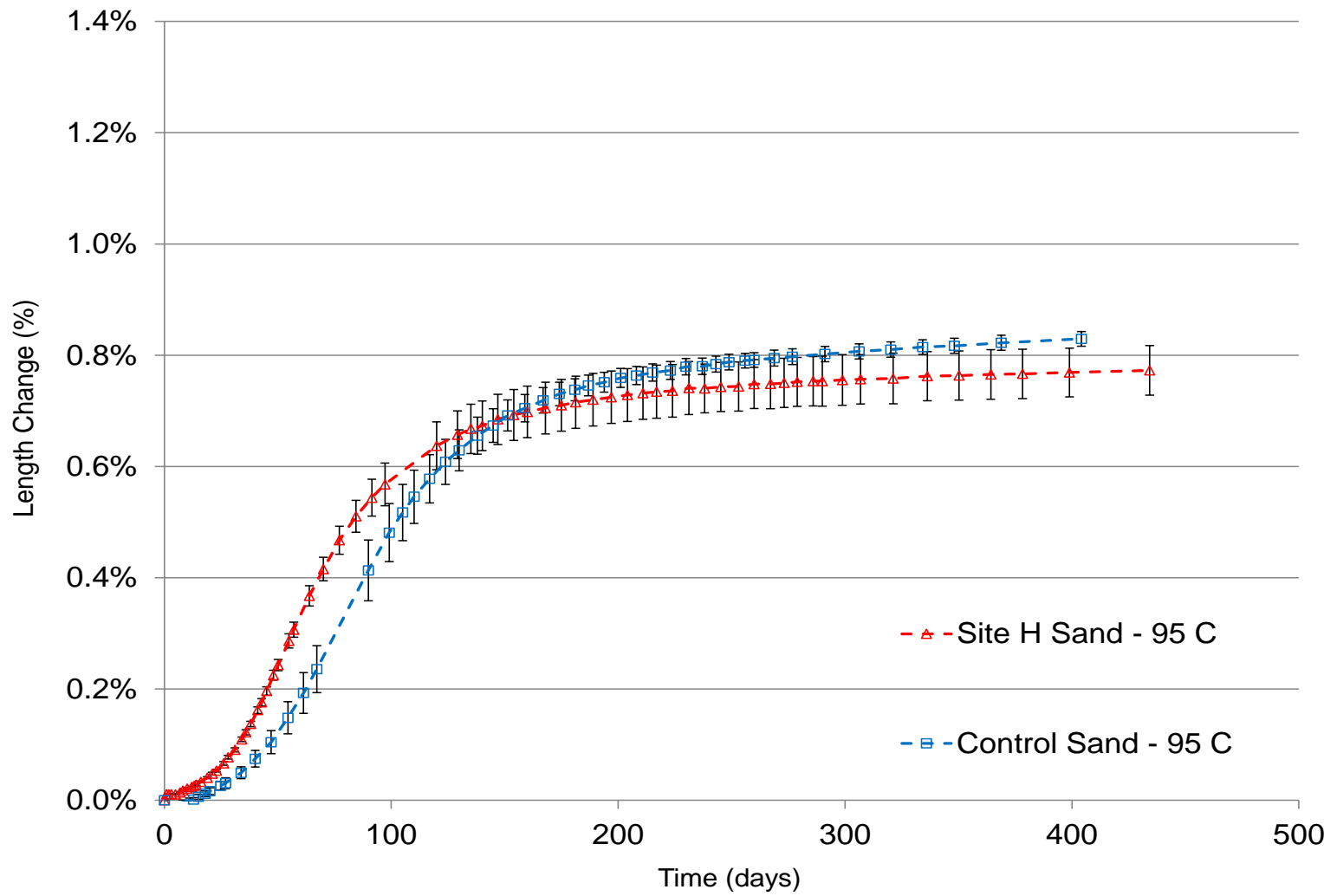


**Figure 6.10.** Expansion of mortar bars due to DEF (Cement A). Error bars represent standard deviation.

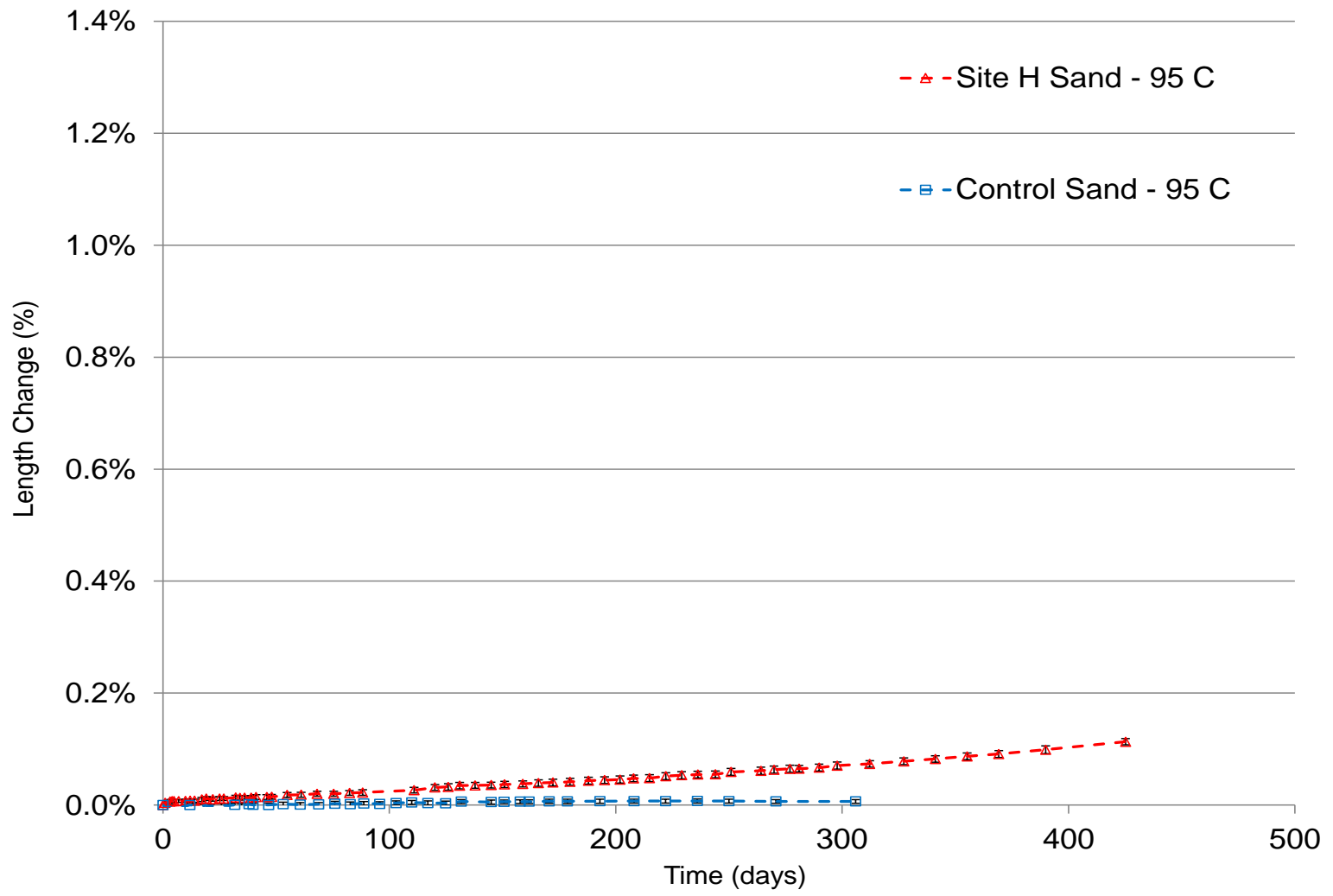


**Figure 6.11.** Expansion of mortar bars due to DEF (Cement B). Error bars represent standard deviation.

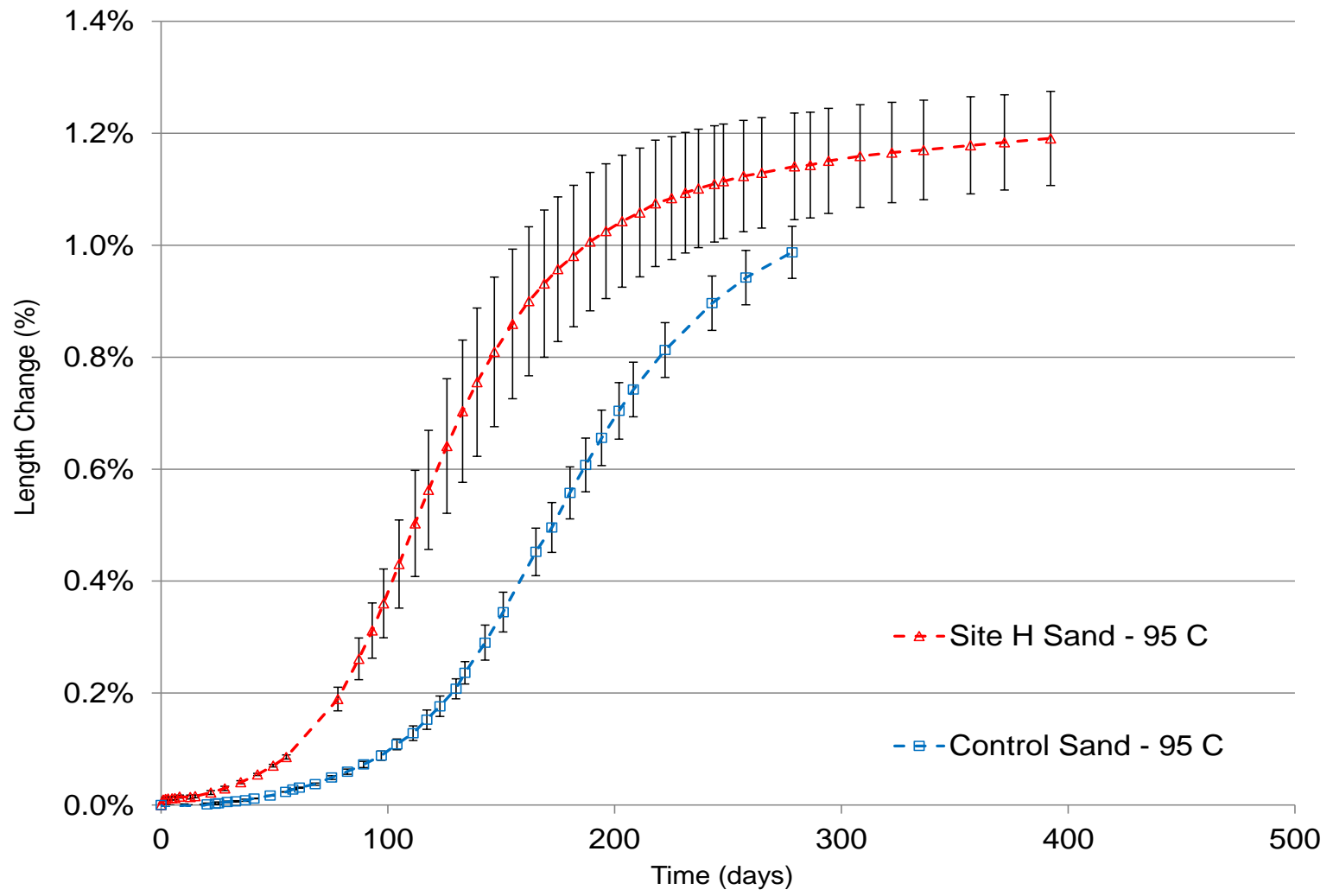


**Figure 6.12.** Expansion of mortar bars due to DEF (Cement C). Error bars represent standard deviation.

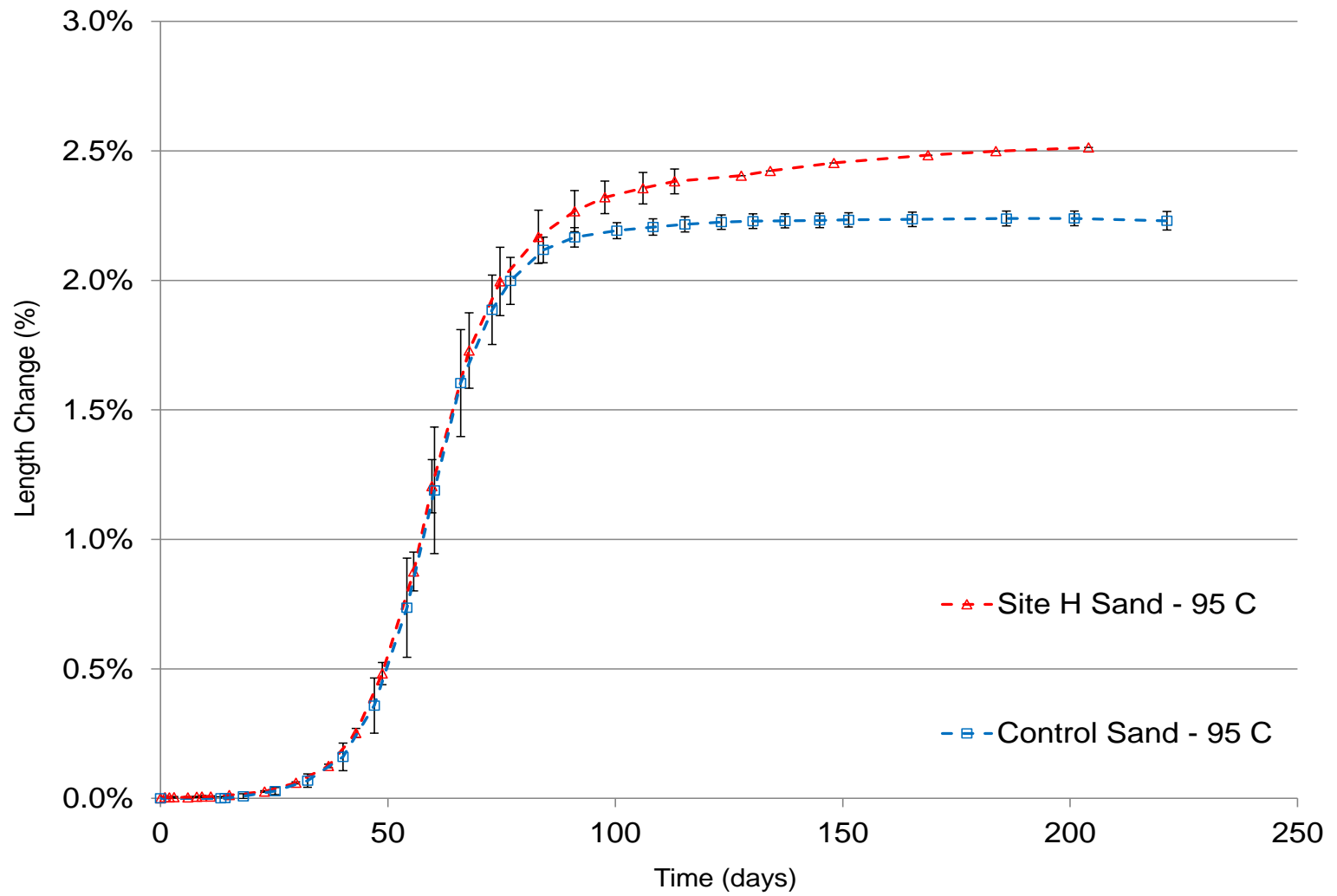


**Figure 6.13.** Expansion of mortar bars due to DEF (Cement D). Error bars represent standard deviation.

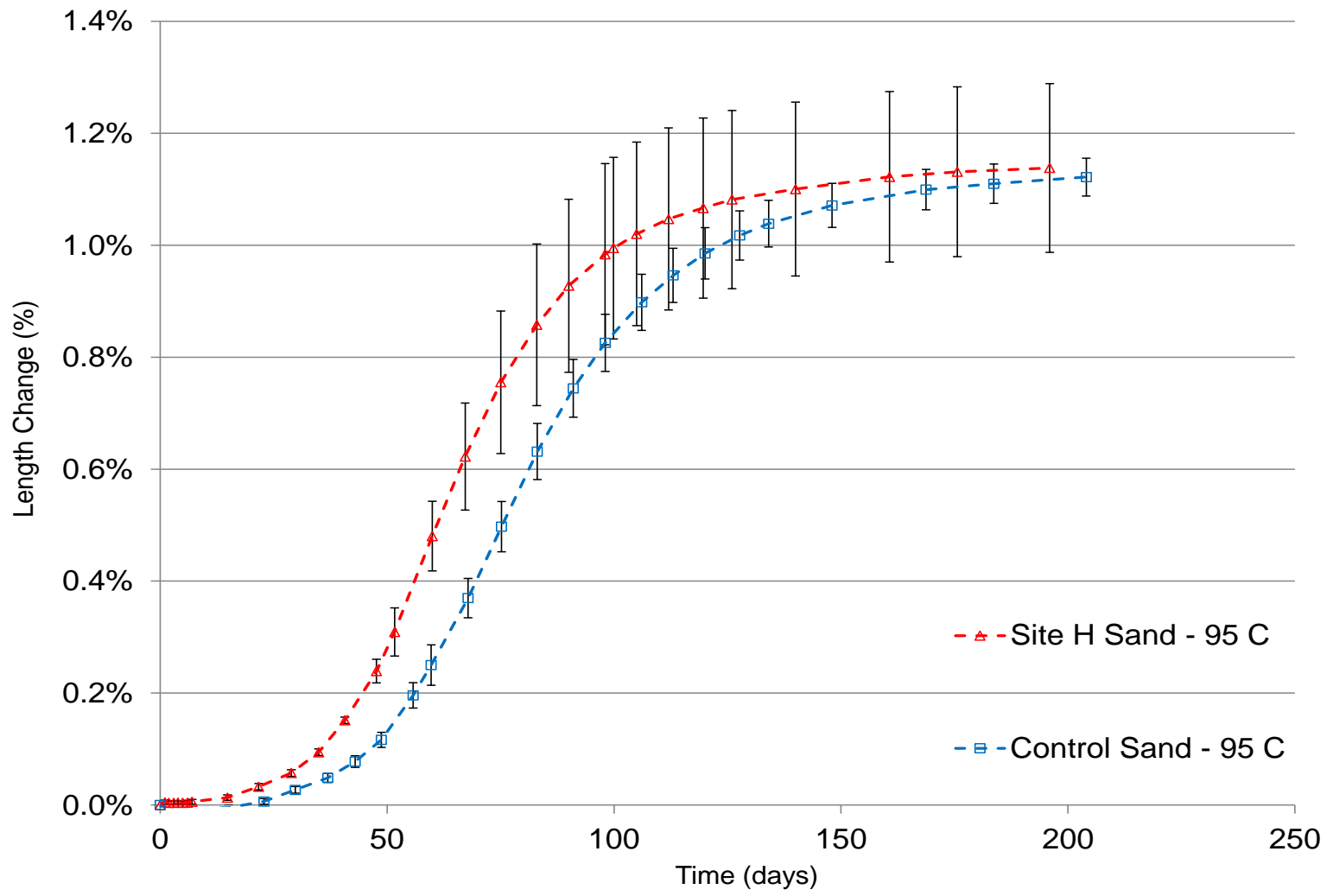


**Figure 6.14.** Expansion of mortar bars due to DEF (Cement E). Error bars represent standard deviation.

In addition to DEF expansion measured in mortar bars, mortar cubes prepared from the same batches were exposed to the same conditions and kept in separate limewater containers. The compressive strength was evaluated at 28 and 100 days from mixing in order to evaluate the effect of the initial curing temperature and the type of sand used in mortar. DEF expansion produces increase of microcracking and sometimes gaps in the paste-aggregate interphase. Consequently, samples affected by significant expansion could show deterioration of the compressive strength.

A summary of the results can be observed in Table 6.3, where it can be seen that the initial high temperature curing produces loss of strength. The application of the Kelham curing cycle to mortar using Cement B and control sand produces a 12% reduction of the strength at 28 days. This difference is incremented for cases where DEF expansion occurred, in samples using Site H sand or control sand and Cement A, C, D, and E. A higher reduction of the strength is appreciable at 100 days when DEF expansion was measured in the corresponding mortar bars.

**Table 6.3.** Compressive strength of cubes at 28 and 100 days from mixing.

Cement	Age of Testing	Mortar mixture	Compressive strength, psi		% of strength at 23 °C
			Average	Std Dev	
Cement A	28 days	Control – 23 °C	<b>6,098</b>	379	
		Control – 95 °C	<b>4,459</b>	330	73.1%
		Site H – 23 °C	<b>6,277</b>	38	
		Site H – 95 °C	<b>4,387</b>	361	69.9%
	100 days	Control – 23 °C	<b>6,418</b>	818	
		Control – 95 °C	<b>4,098</b>	210	63.8%
		Site H – 23 °C	<b>7,547</b>	584	
		Site H – 95 °C	<b>3,924</b>	244	52.0%
Cement B	28 days	Control – 23 °C	<b>6,493</b>	797	
		Control – 95 °C	<b>5,700</b>	417	87.8%
		Site H – 23 °C	<b>6,142</b>	611	
		Site H – 95 °C	<b>5,122</b>	353	83.4%
	100 days	Control – 23 °C	<b>7,620</b>	339	
		Control – 95 °C	<b>6,424</b>	108	84.3%
		Site H – 23 °C	<b>7,502</b>	253	
		Site H – 95 °C	<b>6,161</b>	127	82.1%
Cement C	28 days	Control – 23 °C	<b>7,722</b>	141	
		Control – 95 °C	<b>5,233</b>	429	67.8%
		Site H – 23 °C	<b>7,105</b>	428	
		Site H – 95 °C	<b>5,097</b>	350	71.7%
	100 days	Control – 23 °C	<b>8,455</b>	140	
		Control – 95 °C	<b>5,782</b>	585	68.4%
		Site H – 23 °C	<b>7,868</b>	479	
		Site H – 95 °C	<b>4,498</b>	242	57.2%

**Table 6.3 (cont.).** Compressive strength of cubes at 28 and 100 days from mixing.

Cement	Age of Testing	Mortar mixture	Compressive strength, psi		% of strength at 23 °C
			Average	Std Dev	
Cement D	28 days	Control – 23 °C	<b>6,728</b>	216	
		Control – 95 °C	<b>5,258</b>	130	78.2%
		Site H – 23 °C	<b>7,209</b>	181	
		Site H – 95 °C	<b>4,610</b>	247	63.9%
	100 days	Control – 23 °C	<b>7,255</b>	345	
		Control – 95 °C	<b>2,538</b>	97	35.0%
		Site H – 23 °C	<b>6,854</b>	741	
		Site H – 95 °C	<b>1,830</b>	106	26.7%
Cement E	28 days	Control – 23 °C	<b>6,877</b>	202	
		Control – 95 °C	<b>4,282</b>	242	62.3%
		Site H – 23 °C	<b>6,327</b>	301	
		Site H – 95 °C	<b>4,243</b>	369	67.1%
	100 days	Control – 23 °C	<b>7,667</b>	217	
		Control – 95 °C	<b>3,280</b>	76	42.8%
		Site H – 23 °C	<b>6,893</b>	568	
		Site H – 95 °C	<b>3,570</b>	198	51.8%

In order to better understand the source for mortar expansion, samples from mortar bars prepared using Cement A and Site H sand and cured at high temperature were examined by scanning electron microscopy. Micrographs (Figures 6.15 to 6.17) were produced in a variable pressure SEM (VP-SEM Hitachi S-3700N), at 15 kV, with a working distance of 10 mm, backscattered signal, and chamber pressure of 25 Pa. Also, an EDS elemental point analysis was performed in three regions, as shown in Figure 6.17.

The images show some features commonly associated with DEF-affected concrete or mortar. These include cracking in the paste and gaps around the aggregates, both filled with products which morphologically resemble ettringite. Compositions in regions A-C are summarized in Table 6.4. The higher S/Ca and Al/Ca of regions A and B are most consistent with the presence of ettringite [Tosun and Baradan, 2010].

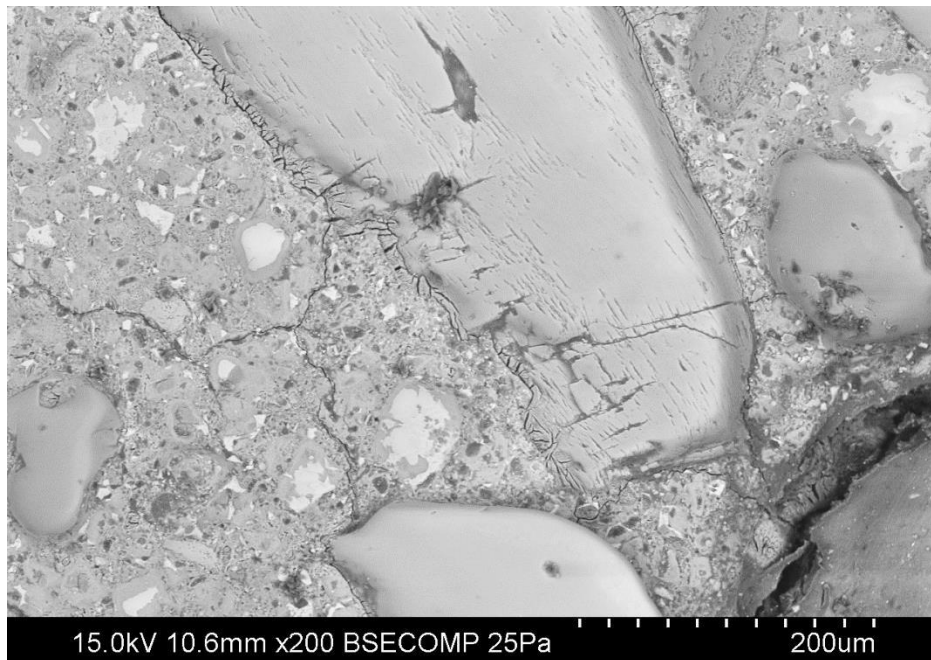


**Figure 6.15.** Backscattered micrograph of a DEF-affected mortar sample (200 X).

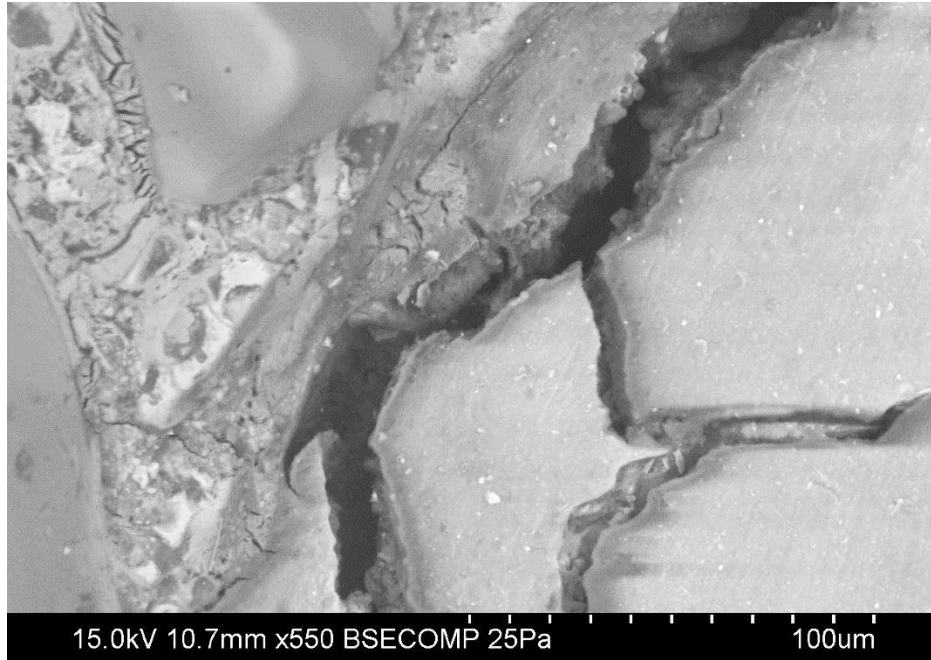


**Figure 6.16.** Backscattered micrograph of a DEF affected mortar sample (550 X).



**Figure 6.17.** Backscattered micrograph of a DEF affected mortar sample (1,400 X).

**Table 6.4.** EDS point analysis over regions A, B, and C of Figure 6.17.

<b>Element</b>	<b>A</b>		<b>B</b>		<b>C</b>	
	Weight %	Atomic %	Weight %	Atomic %	Weight %	Atomic %
<b>C</b>	16.52	24.46	27.91	38.30	28.11	37.67
<b>O</b>	54.37	60.42	48.51	49.98	53.15	53.49
<b>Mg</b>	0.19	0.14	0.42	0.29	0.47	0.31
<b>Al</b>	3.89	2.56	2.74	1.68	0.99	0.59
<b>Si</b>	3.94	2.49	6.49	3.81	5.78	3.31
<b>S</b>	5.03	2.79	2.15	1.10	0.28	0.14
<b>K</b>	0.85	0.39	1.13	0.48	0.26	0.11
<b>Ca</b>	15.21	6.75	10.64	4.38	10.72	4.31
<b>Fe</b>					0.25	0.07
<b>S/Ca</b>	0.331	0.413	0.202	0.251	0.026	0.032
<b>Al/Ca</b>	0.256	0.379	0.258	0.384	0.092	0.137

## 7. CONCLUSIONS AND RECOMMENDATIONS

The use of sulfide- and sulfate-bearing aggregates in concrete and mortar was found to produce measureable effects on early age behavior, mechanical properties, and factors influencing long-term performance. Both acidic sands tested behaved in a different way with respect to a GDOT-approved sand used as a control. Furthermore, sands obtained from the same deposit, at different times, also presented dissimilar performance in terms of early-age and mechanical properties. These results evidence the variability of the sand deposit and the lack of consistency of the extracted sand.

### 7.1 Conclusions

- Isothermal calorimetry results show that for a range of cement compositions delays in early cement hydration can be expected in the presence of Site D or Site H sand, compared to the GDOT-approved sand source. The magnitude of the delay is dependent on the cement composition and the sand, with Site H producing generally greater delays, presumably due to a greater sulfate content in that source.

- The setting time was tested for a single Type I/II cement, and the use of acidic sands delays the initial and final times of setting compared to control sand. Site H sand showed greater delay, up to 85 minutes, in setting time.

- Comparing slump and air content in AA1 concrete produced with each of the three sand sources showed that Site H sand lead to lower slump values and lower air

contents. It is not clear if these effects are related to the greater fineness of the Site H sand or its higher sulfate/sulfide content or a combination of these effects.

- A moderate increase in compressive strength and dynamic modulus of elasticity is observed in concrete containing Site H sand when compared to that with control sand or Site D sand, when examined in GDOT Class AA1 concrete. Statistical analysis shows that the compressive strength and dynamic modulus of Site H concrete are higher compared to Site D samples, at every age of testing. Despite the higher values obtained for the Site H concrete, because Site D and H sand were obtained from the same source, the variability in the concrete mechanical properties is a concern.

- All sands produced AA1 concretes with 56-day rapid chloride permeability results in the moderate range.

- When examining the potential for the Site H sand to participate in reactions leading to DEF-induced expansion in mortar mixtures exposed to a high temperature curing, dependence on cement composition was noted. For Type I, I/II, and III cements, the presence of Site H sand accelerates the onset and rate of DEF expansion. Expansions with Site H sand combined with Type V cement were negligible during the test period examined, although still greater than for the same cement combined with the control sand.

- No evidence of expansion due to internal sulfate attack initiated by the presence of sulfates or sulfides in the aggregate sources was observed in mortar samples over the testing period examined.

- The use of the Site H and Site D sands lead to earlier corrosion of the reinforced steel bars compared to control sands, in concrete. The initiation of active corrosion

occurred at an earlier age, and a more extensive cracking and damage due to corrosion was observed when the Site D or H sands were used.

## **7.2 Recommendations**

1. Coastal lowland sources of aggregates should be tested in order to identify contamination by sulfates, sulfides or other potentially deleterious components and to assess pH. Testing should be performed routinely, to quantify variations in the same source or stockpile over time and variations during production and storage.
2. Due to concerns related to DEF, the use of the analyzed sand deposit, where both Site D and Site H sands were obtained, is not recommended for mass, prestressed concrete, precast operations, or other applications where early high temperature could produce DEF, unless Type V cement is used in the mixture composition. The use of supplementary cementitious materials (SCMs) may provide some benefit when general use cements must be used, but the appropriate SCM type and use rate must be established.
3. The analyzed sand deposit, where both Site D and Site H sands were obtained, is not recommended for marine environments, given that concrete containing acidic sands is more prone to corrosion. This is particularly sensible in the case of prestressed concrete elements, where the chloride threshold limit (CTL) is lower due to the presence of crevices located at the impingement sites between adjoining prestressing wires. Prior guidance [Holland, 2012] has been provided on the use of ASTM C150 Type II cement, in combination with fly ash or slag, for

durable marine construction, and these recommendations may be used to guide the development and assessment of concrete for reinforced elements in marine environments.

4. For applications where consistency in setting time, slump, or air content is critical, the analyzed sand deposit, where both Site D and Site H sands were obtained, is not recommended.<sup>3</sup>

### 7.3 Future Needs

The results obtained through this limited research effort show the need to extend the work on acidic and sulfate/sulfide-bearing sands, in particular because this topic has not been well-addressed in the literature or current codes. There is growing awareness of the importance of such materials, however. For example, ACI Committee 201 on Durability recently identified this topic as one to be addressed by a newly formed task group on aggregate reactivity. ACI 201 plans to include guidance on sulfate- and sulfide-bearing aggregates in future version of 201.2R Guide to Durable Concrete.

Improved understanding of the implications of sulfate and sulfide contents, as well as low pH, on concrete properties is needed. Additional research should address:

---

<sup>3</sup> However, with appropriate adjustments in chemical admixture use, it may be possible to overcome these effects. Further effort will be necessary to better understand the variability in behavior and appropriate admixture dosages or range of dosages to compensate for variations in performance due to sand composition.

- Quantification of the composition and variation in composition of sand deposits in the coastal region in the state to establish their range and variability.

- Statistical analysis, for a range of sands and a range of concrete compositions with varying binder (i.e., cement and SCM) compositions, to appreciate the range of mechanical behavior to better appreciate the influence of the inconsistency of sand source.

- The combination of cements with SCMs such as fly ash, silica fume or metakaolin, for the mitigation of DEF to determine appropriate SCMs compositions and their level of cement replacement. Currently, there is limited research showing the efficiency of SCM replacement in order to reduce or avoid expansion.

- Further examination of the influence of sand source on permeability and chloride ion migration is needed.

- The effect of the use of cement Type V on the corrosion resistance of reinforced concrete should be analyzed. Friedel's salt formation product of the reaction of  $C_3A$  and chloride ions could be minimized in the case of Type V cement. As a result, an even lower corrosion resistance could be obtained.

- Further analyses of the expansion results of additional cements (here labeled Cement D and E) should give more information about the influential factors that determine DEF occurrence, the amount of DEF expansion, and the onset of the accelerated expansion process.

## REFERENCES

- Al-Rawi, R.S., Al-Salihi, R.A.W., Ali, M.H.M., 2002, "Effective Sulfate Content in Concrete Ingredients," in: R.K. Dhir (Ed.), *Challenges of Concrete Construction: Volume 6, Concrete for Extreme Conditions*, Thomas Telford Ltd, pp. 499–506.
- Atahan, H.N., Dikme, D., 2010, "Improving Sulfate Resistance of Mortars Produced with Sands Contaminated by Natural Sulfate," in: W. Brameshuber (Ed.), *International RILEM Conference on Material Science*, RILEM Publications SARL.
- Atahan, H.N., Dikme, D., 2011, Use of mineral admixtures for enhanced resistance against sulfate attack, *Construction and Building Materials* 25:3450-3457.
- Attiogbe, E.K., Rizkalla, S.H., 1988, Response of Concrete to Sulfuric Acid Attack, *ACI Materials Journal* 85 (6), 481–488.
- Beddoe, R.E., Dorner, H.W., 2005, Modelling Acid Attack on Concrete: Part I. The Essential Mechanisms, *Cement and Concrete Research* 35 (12), 2333–2339.
- Bensted, J., 1982, in: J.F. Young (Ed.), *Characterization and Performance Prediction of Cement and Concrete*, Proceedings of the Second Engineering Foundation Conference, Henniker, NH, p. 69.
- Berner, R.A., 1984, Sedimentary Pyrite Formation: An Update, *Geochimica et Cosmochimica Acta* 48 (4), 605–615.
- Bogue, R.H., 1947. *The Chemistry of Portland Cement*, New York: Reinhold Publishing Corp.
- Böttcher, M.E., 2011, "Sulfur Cycle," in: V. Reitner, J. Thiel (Eds.), *Encyclopedia of Geobiology*, Springer: Heidelberg, pp 856.

- Brimblecombe, P., 2003, "The global sulfur cycle," in W. Schlesinger (Ed.), *Treatise on Geochemistry, Biogeochemistry*. Elsevier: Amsterdam, Vol. 8, pp. 645.
- Chandra, A.P., Gerson, A.R., 2010, *The Mechanisms of Pyrite Oxidation and Leaching: A Fundamental Perspective*, *Surface Science Reports* 65 (9), 293–315.
- Chinchón-Payá, S., Aguado, A., Chinchón, S., 2012, *A Comparative Investigation of the Degradation of Pyrite and Pyrrhotite under Simulated Laboratory Conditions*, *Engineering Geology* 127 (24), 75–80.
- Ekolu, S.O., Thomas, M.D.A., Hooton, R.D., 2006, *Pessimism Effect of Externally Applied Chlorides on Expansion Due To Delayed Ettringite Formation: Proposed Mechanism*, *Cement and Concrete Research* 36 (4), 688–696.
- Fitzpatrick, R.W., Shand, P., Merry, R.H., 2009, "Acid Sulfate Soils," in: J.T. Jennings (Ed.), *Natural History of the Riverland and Murraylands*, Royal Society of South Australia: Adelaide, Australia, pp 65–111.
- Flatt, R.J., Scherer, G.W., 2008, *Thermodynamics of Crystallization Stresses in DEF*, *Cement and Concrete Research* 38 (3), 325–336.
- Florida DOT, 2000, *An Accelerated Laboratory Method for Corrosion Testing of Reinforced Concrete Using Impressed Current*, FM 5-522, Tallahassee, FL.
- Folliard, K.J., Barborak, R., Drimalas, T., Du, L., Garber, S., Ideker, J., Ley, T., Williams, S., Juenger, M., Fournier, B., Thomas, M.D.A., 2006, *Preventing ASR/DEF in new concrete: Final report*. Center for Transportation Research, The University of Texas at Austin, Report 0-4085-5, Austin, TX.
- Glasser, F.P., 2002, *The stability of ettringite*, *Proceedings of RILEM Meeting on Delayed Ettringite Formation*, Villars-sur-Ollon, Switzerland, Sept. 4–6.

- Hails, J.R., Hoyt, J.H., 1969, An Appraisal of the Evolution of the Lower Atlantic Coastal Plain of Georgia, USA, Transactions of the Institute of British Geographers 46, 53–68.
- Hansson, C.M., 1984, Comments on Electrochemical Measurements of the Rate of Corrosion of Steel in Concrete, Cement and Concrete Research 14 (4), 574–584.
- Hawkins, A.B., 2014, “Engineering Implications of the Oxidation of Pyrite: An Overview, with Particular Reference to Ireland,” in: A.B. Hawkins (Ed.), Implications of Pyrite Oxidation for Engineering Works, Springer International Publishing: Switzerland.
- Herrick, S.M., Vorhis, R.C., 1963, Subsurface Geology of the Georgia Coastal Plain, The Geological Survey, Information Circular 25.
- Holland, R.B., Moser, R., Kahn, L., Singh, P. and Kurtis, K., 2012, “Durability of Precast Prestressed Piles in Marine Environment, Part 2; Volume 1: Concrete”, Final Report, Georgia Department of Transportation, Forest Park, GA. Available at <http://www.dot.ga.gov/doingbusiness/research/Documents/GDOT%20RP%2010-26%20Final%20Report%20Pile%20Durability%20Part%202%20Vol%201.pdf>
- Jayapalan, A.R., Jue, M.L., Kurtis, K.E., 2014, Nanoparticles and Apparent Activation Energy of Portland Cement, Journal of the American Ceramic Society 97 (5), 1534–1542.
- Jones, D.A., 1995, Principles and Prevention of Corrosion, Second Edition, Prentice Hall.
- Kelham, S., 1997, Effects of cement composition and hydration temperature on volume stability of mortar, Proceeding of the 10th International Congress on the Chemistry of Cement, vol. 4, Amarkai AB and Congrex, Gothenburg, Sweden, 8 pp, 4iv060.
- Kheder, G.F., Assi, D.K., 2010, Limiting Total Internal Sulphates in 15-75 MPa Concrete in Accordance to Its Mix Proportions, Materials and Structures 43 (1–2), 273–281.

- Mehta, P.K., Monteiro, P.J.M., 2006. *Concrete: Microstructure, Properties and Materials*, Third Edition, McGraw-Hill.
- Mindess, S., Young, J.F., Darwin, D., 2003. *Concrete*, Prentice Hall: Upper Saddle River, NJ.
- Monteny, J., Vincke, E., Beeldens, A., De Belie, N., Taerwe, L., Van Gemert, D., Verstraete, W., 2000, Chemical, Microbiological, and In Situ Test Methods for Biogenic Sulfuric Acid Corrosion of Concrete, *Cement and Concrete Research* 30 (4), 623–634.
- Moser, R.D., Singh, P.M., Kahn, L.F., Kurtis, K.E., 2011, Chloride-Induced Corrosion of Prestressing Steels Considering Crevice Effects and Surface Imperfections, *Corrosion* 67, 1–14.
- Neville, A., 2004, The Confused World of Sulfate Attack on Concrete, Cement and Concrete Research 34 (8), 1275–1296.
- Nordstrom, D.K., Southam, G., 1997, “Geomicrobiology of Sulfide Mineral Oxidation,” in: J.F. Banfield, K.H. Nealson (Eds.), *Geomicrobiology: Interactions Between Microbes and Minerals*, Vol. 35, *Reviews in Mineralogy*, Washington, DC: Mineralogical Society of America, pp 361–390.
- Nordstrom, D.K., 2011, “Sulfide Mineral Oxidation,” in: V. Reitner, J. Thiel (Eds.), *Encyclopedia of Geobiology*, Springer: Heidelberg, pp 856.
- Pavoine, A., Brunetaud, X., Divet, L., 2012, The Impact of Cement Parameters on Delayed Ettringite Formation, *Cement and Concrete Composites* 34 (4), 521–528.
- Petrov, N., Tagnit-Hamou, A., 2004, Is Microcracking Really a Precursor to Delayed Ettringite Formation and Consequent Expansion?, *ACI Materials Journal* 101 (6), 442–447.

- Popovics, J.S., Zemajtis, J., Shkolnik, I., 2008, A Study of Static and Dynamic Modulus of Elasticity of Concrete, ACI-CRC Final Report.
- Rickard, D., Luther, G.W., 2007, Chemistry of Iron Sulfides, *Chemical Reviews* 107 (2), 514–562.
- Santhanam, M., Cohen, M.D., Olek, J., 2001, Sulfate Attack Research – Whiter Now?, *Cement and Concrete Research* 31 (6), 845–851.
- Schindler, A.K., Folliard, K.J., 2005, Heat of Hydration Models for Cementitious Materials, *ACI Materials Journal* 102 (1), 24–33.
- Schmidt, T., Leemann, A., Gallucci, E, Scrivener, K., 2011, Physical and Microstructural Aspects of Iron Sulfide Degradation in Concrete, *Cement and Concrete Research* 41 (3), 263–269.
- Scrivener, K., Skalny, J.P., 2005, Conclusions of the International RILEM TC 186-ISA Workshop on Internal Sulfate Attack and Delayed Ettringite Formation (4-6 September 2002, Villars, Switzerland), *Materials and Structures* 38 (6), 659–663.
- Taylor, H.F.W., 1997. *Cement Chemistry*, 2nd Edition, Thomas Telford.
- Taylor, H.F.W., Famy, C., Scrivener, K.L., 2001, Delayed Ettringite Formation, *Cement and Concrete Research* 31 (5), 683–693.
- Thomas, M.D.A., Folliard, K., Drimalas, T., Ramlochan, T., 2006, Diagnosing Delayed Ettringite Formation in Concrete Structures, *Cement and Concrete Research* 36 (4), 688–696.
- Thomas, M.D.A., Ramlochan, T., 2004, Field Cases of Delayed Ettringite, in: K. Scrivener, J. Skalny (Eds.), *Proceedings of an International RILEM Workshop on Internal Sulfate Attack and Delayed Ettringite Formation*, RILEM Publications SARL, 85–97.

- Tosun, K., Baradan, B., 2010, Effect of Ettringite Morphology on DEF-related Expansion, *Cement and Concrete Composites* 32 (4), 271–280.
- Tovar-Rodríguez, G., Barra, M., Pialarissi, S., Aponte, D., Vázquez E., 2013, Expansion of Mortars with Gypsum Contaminated Fine Recycled Aggregates, *Construction and Building Materials* 38, 1211–1220.
- Tsuneyuki, S., Aoki, H., Tsukada, M., Matsui, Y., 1990, Molecular-Dynamics Study of the  $\alpha$  to  $\beta$  Structural Phase Transition of Quartz, *Physical Review Letters* 64 (7), 776–779.
- Zein Al-Abidien, H.M., 1987, Aggregates in Saudi Arabia: A Survey of Their Properties and Suitability for Concrete, *Materials and Structures* 20 (4), 260–264.

**APPENDIX A: Modeled Degree of Hydration on Time.**

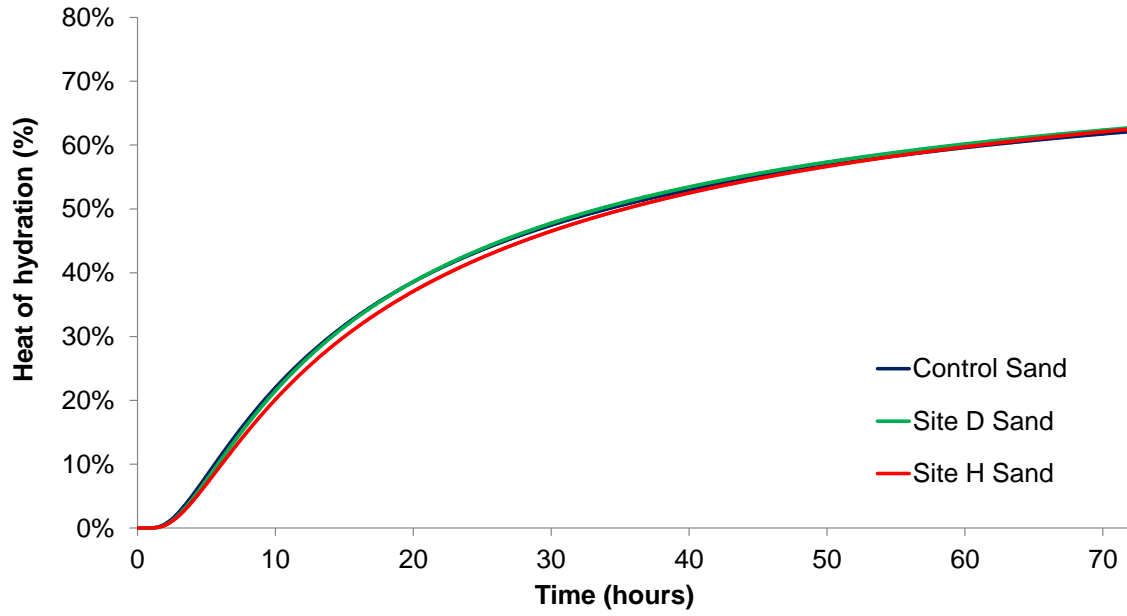


**Figure A.1.** Degree of hydration for mortars using Cement A.

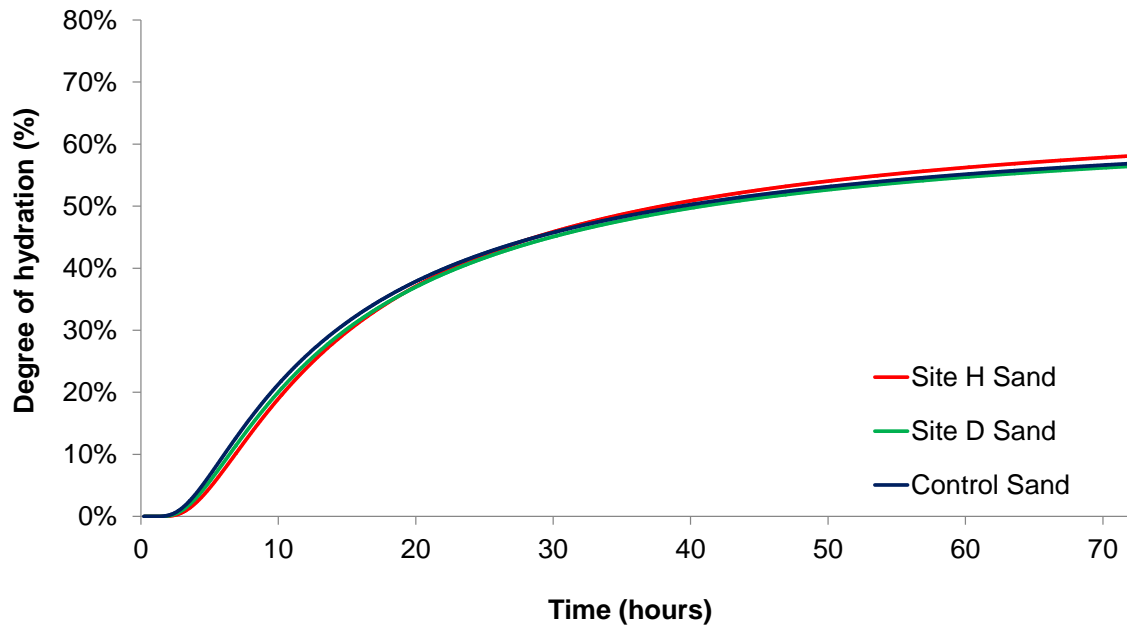


**Figure A.2.** Degree of hydration for mortars using Cement B.

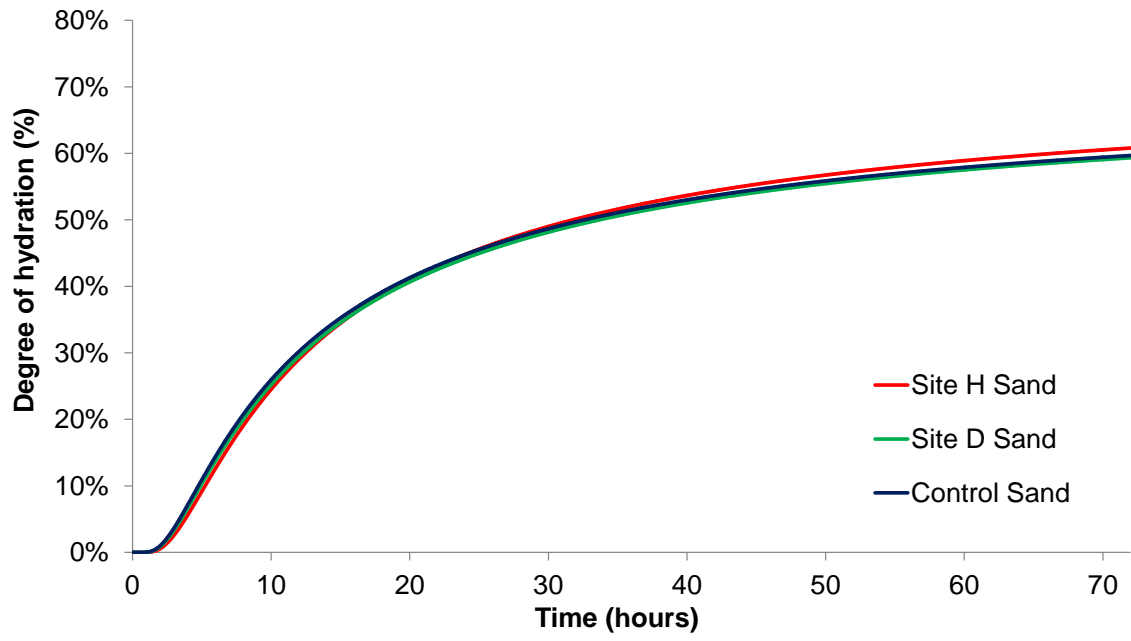


**Figure A.3.** Degree of hydration for mortars using Cement C.

## APPENDIX B: Individual Results of Compressive Strength of Concrete

**Table B.1.** Individual results of compressive strength test for control sand specimens.

	Age	Compressive Strength (psi)	Rounded Compressive Strength (psi)	Average (psi)	Standard Deviation (psi)
<b>CONTROL SAND</b>	1 day	2,428.8	2,430	<b>2,533</b>	280
		2,324.2	2,320		
		2,847.5	2,850		
	3 days	3,192.6	3,190	<b>3,137</b>	76
		3,052.6	3,050		
		3,168.8	3,170		
	7 days	5,171.7	5,170	<b>4,850</b>	288
		4,765.9	4,770		
		4,613.9	4,610		
	28 days	4,835.9	4,840	<b>5,533</b>	621
		5,720.0	5,720		
		6,039.9	6,040		
	56 days	5,480.5	5,480	<b>5,797</b>	275
		5,966.7	5,970		
		5,940.5	5,940		
	90 days	6,407.6	6,410	<b>6,233</b>	159
		6,098.8	6,100		
		6,186.4	6,190		

**Table B.2.** Individual results of compressive strength test for Site H sand specimens.

	Age	Compressive Strength (psi)	Rounded Compressive Strength (psi)	Average (psi)	Standard Deviation (psi)
<b>SITE H SAND</b>	1 day	3,604.1	3,600	<b>3,650</b>	87
		3,602.5	3,600		
		3,750.5	3,750		
	3 days	4,006.7	4,000	<b>4,123</b>	188
		4,033.8	4,030		
		4,343.3	4,340		
	7 days	5,104.9	5,100	<b>5,480</b>	344
		5,566.4	5,570		
		5,766.2	5,770		
	28 days	6,642.3	6,640	<b>6,637</b>	55
		6,584.2	6,580		
		6,689.3	6,690		
	56 days	7,188.2	7,190	<b>7,670</b>	423
		7,991.2	7,990		
		7,832.0	7,830		
	90 days	-----	wrong failure	<b>7,895</b>	92
		7,832.0	7,830		
		7,960.9	7,960		

**Table B.3.** Individual results of compressive strength test for Site D sand specimens.

	Age	Compressive Strength (psi)	Rounded Compressive Strength (psi)	Average (psi)	Standard Deviation (psi)
<b>SITE D SAND</b>	1 day	2,819.4	2,820	<b>2,590</b>	252
		2,324.5	2,320		
		2,633.2	2,630		
	3 days	3,775.2	3,780	<b>3,557</b>	225
		3,325.5	3,330		
		3,561.1	3,560		
	7 days	4,221.6	4,220	<b>4,447</b>	575
		4,018.7	4,020		
		5,103.3	5,100		
	28 days	5,552.9	5,550	<b>5,647</b>	249
		5,928.5	5,930		
		5,457.4	5,460		
	56 days	6,835.7	6,840	<b>6,710</b>	225
		6,449.8	6,450		
		6,836.5	6,840		
	90 days	6,659.8	6,660	<b>6,790</b>	184
		6,920.9	6,920		
		-----	wrong failure		

### APPENDIX C: Variability of Results - Accelerated Corrosion Testing

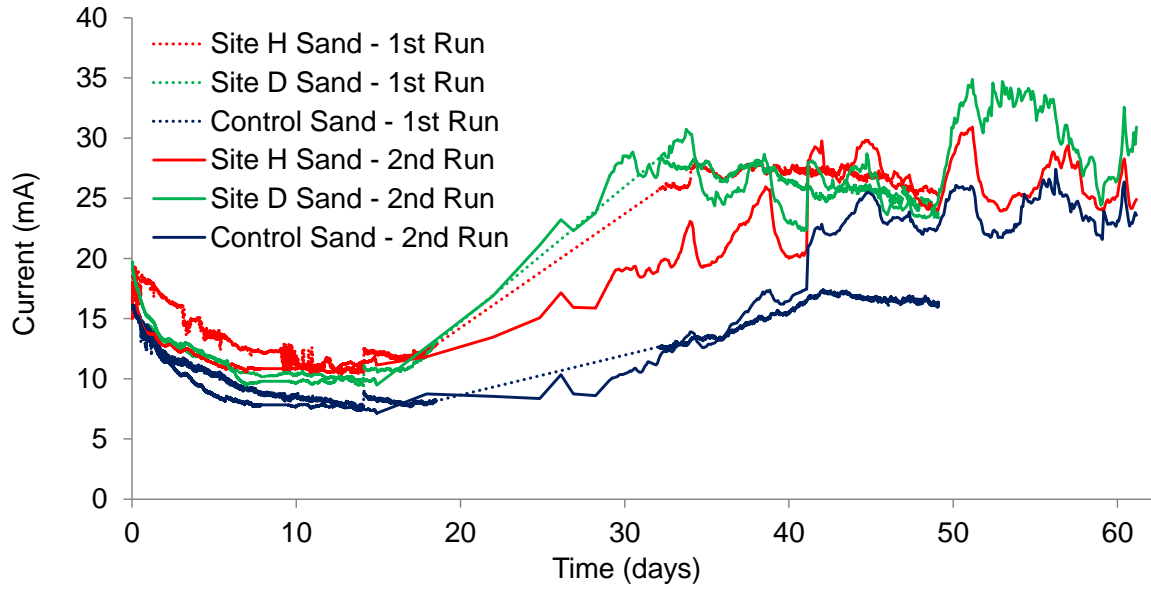


**Figure C.1.** Evolution of current during the test for concrete specimens.

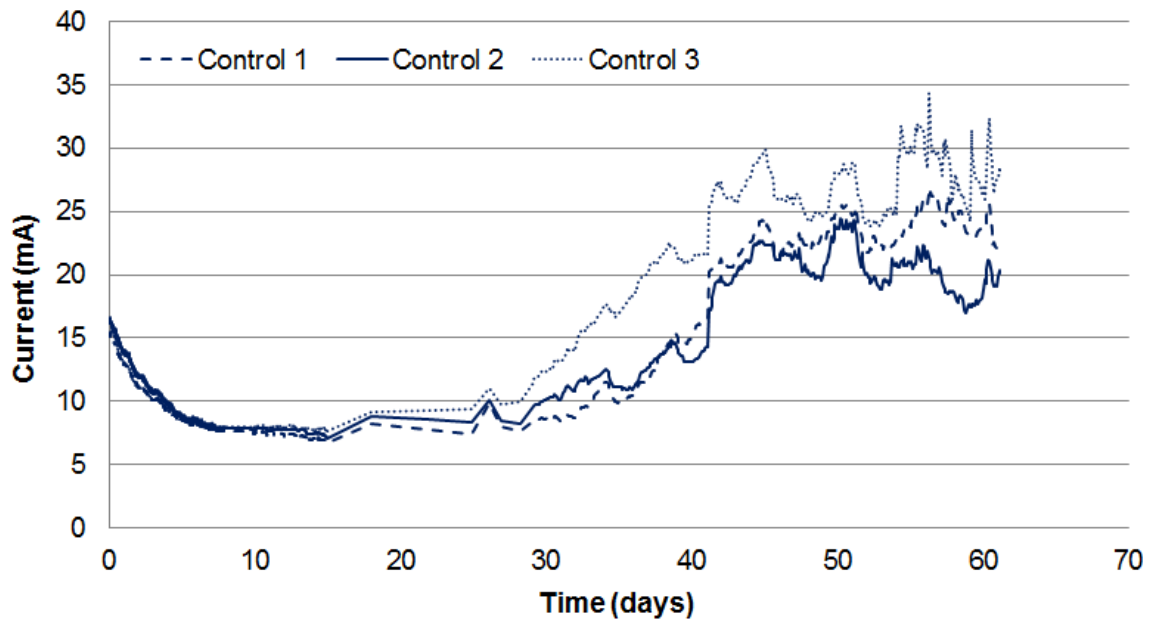


**Figure C.2.** Evolution of current during the test for control sand specimens.

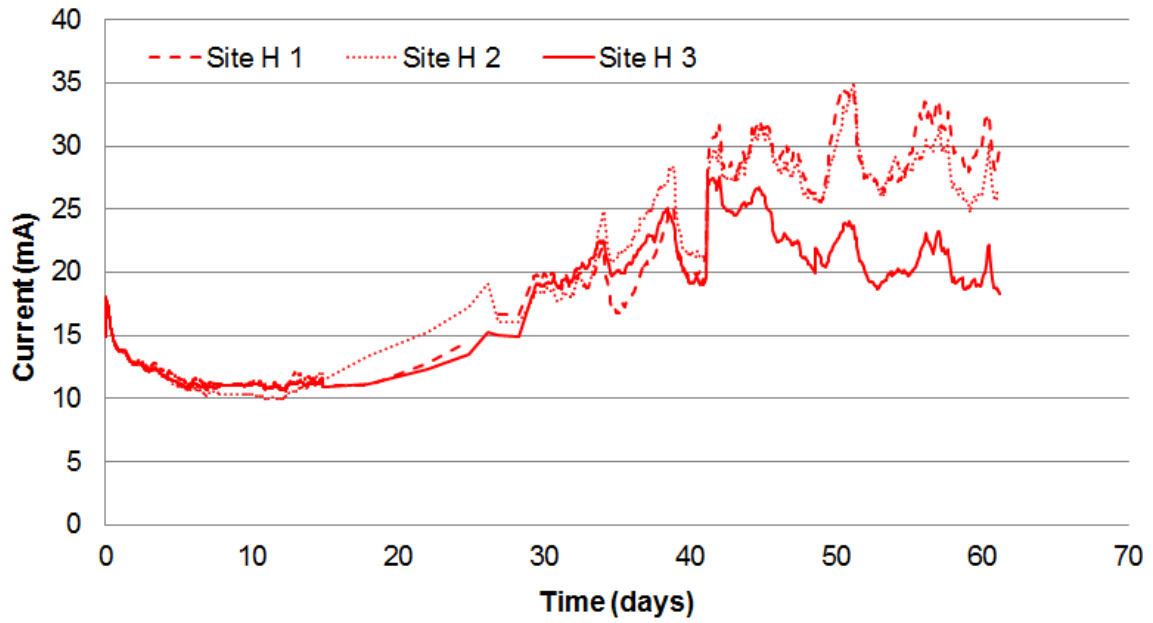


**Figure C.3.** Evolution of current during the test for Site H sand specimens.

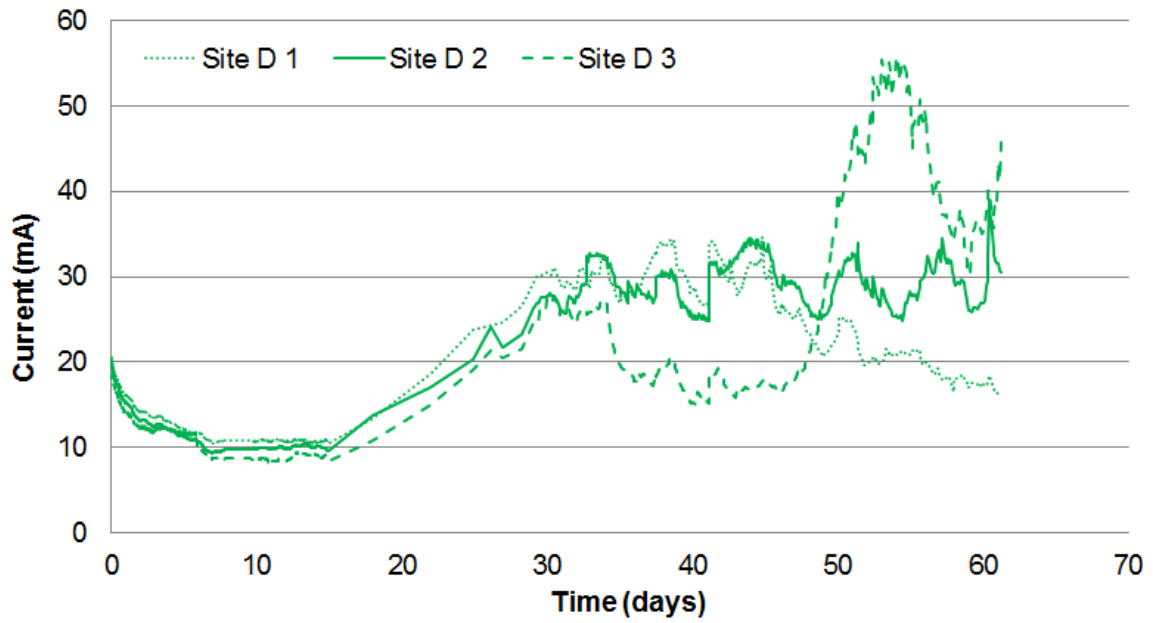


**Figure C.4.** Evolution of current during the test for Site D sand specimens.